



# Ice properties of single-layer stratocumulus during the Mixed-Phase Arctic Cloud Experiment:

## 2. Model results

A. M. Fridlind,<sup>1</sup> A. S. Ackerman,<sup>1</sup> G. McFarquhar,<sup>2</sup> G. Zhang,<sup>2</sup> M. R. Poellot,<sup>3</sup> P. J. DeMott,<sup>4</sup> A. J. Prenni,<sup>4</sup> and A. J. Heymsfield<sup>5</sup>

Received 9 March 2007; revised 24 August 2007; accepted 20 September 2007; published 20 December 2007.

[1] Measurements from the US Department of Energy Atmospheric Radiation Measurement Program's 2004 Mixed-Phase Arctic Cloud Experiment (M-PACE) provide a unique opportunity to study poorly understood ice formation processes in mixed-phase stratocumulus. Using meteorological, aerosol, and ice nucleus measurements to initialize large-eddy simulations with size-resolved microphysics, we compare predicted liquid and ice mass, number, and size distribution with observations from a typical flight. We find that ambient ice nuclei appear insufficient by a few orders of magnitude to explain observed ice, consistent with past literature. We also find that two processes previously hypothesized to explain the discrepancy, shatter of freezing drops and fragmentation during ice-ice collisions, were not significant sources of ice based on parameterizations from existing studies. After surveying other mechanisms that have been hypothesized to explain ice formation in mixed-phase clouds generally, we find two that may be strong enough: (1) formation of ice nuclei from drop evaporation residuals, a process suggested by sparse and limited measurements to date, and (2) drop freezing during evaporation, a process suggested only by inference at this time. The first mechanism can better explain the persistence of mixed-phase conditions in simulations of less vigorous stratus observed during the Beaufort Arctic Storms Experiment (BASE). We consider conditions under which emission of nuclei from the ocean surface or activation through cloud-phase chemistry could provide alternative explanations for M-PACE observations. Additional process-oriented measurements are suggested to distinguish among ice formation mechanisms in future field studies.

**Citation:** Fridlind, A. M., A. S. Ackerman, G. McFarquhar, G. Zhang, M. R. Poellot, P. J. DeMott, A. J. Prenni, and A. J. Heymsfield (2007), Ice properties of single-layer stratocumulus during the Mixed-Phase Arctic Cloud Experiment: 2. Model results, *J. Geophys. Res.*, 112, D24202, doi:10.1029/2007JD008646.

## 1. Introduction

[2] In response to a growing recognition of the inadequacy of existing observations to correct evident errors in the representation of Arctic physical processes in general circulation models, the US Department of Energy (DOE) Atmospheric Radiation Measurement (ARM) Program located one of its primary long-term measurement sites at the North Slope of Alaska (NSA), placing an emphasis on observation of clouds, radiation, and water vapor [*Curry et*

*al.*, 1996; *Randall et al.*, 1998]. Routine ground-based measurements began there in 1998, with the goal of later performing extended domain studies around the site with additional instrumentation to study cloud processes [*Stamnes et al.*, 1999]. From late September through late October of 2004, the Mixed-Phase Arctic Cloud Experiment (M-PACE) was conducted as one of the ARM Program's Intensive Observation Periods (IOPs) at the NSA site, including enhanced measurements from three airborne platforms and three additional ground sites [*Verlinde et al.*, 2007].

[3] During 9–12 October of the M-PACE campaign, a widespread supercooled boundary layer stratocumulus deck persisted over the region, with cloud layer temperatures of about  $-8.5$  to  $-15.5^{\circ}\text{C}$  [*Verlinde et al.*, 2007; *McFarquhar et al.*, 2007]. Although conditions were unseasonably warm, and the degree of glaciation therefore lower than expected, extensive observations of aerosols, ice nuclei, cloud properties, and meteorological conditions were nonetheless obtained in the stratocumulus deck under mixed-phase conditions, thus meeting a primary goal of the experiment.

<sup>1</sup>NASA Goddard Institute for Space Studies, New York, New York, USA.

<sup>2</sup>Department of Atmospheric Sciences, University of Illinois, Urbana, Illinois, USA.

<sup>3</sup>Department of Atmospheric Sciences, University of North Dakota, Grand Forks, North Dakota, USA.

<sup>4</sup>Department of Atmospheric Science, Colorado State University, Fort Collins, Colorado, USA.

<sup>5</sup>National Center for Atmospheric Research, Boulder, Colorado, USA.

Part 1 of this two-part paper describes the integrative processing of cloud measurements from a range of instruments that was required to improve estimation of the stratocumulus properties, such as ice crystal number and size distribution under mixed-phase conditions [McFarquhar *et al.*, 2007]. Here we describe our use of a subset of the processed in situ cloud data, in conjunction with aerosol and meteorological measurements, to evaluate the ability of numerical simulations to reproduce the observed clouds. Since ice formation mechanisms emerged as the greatest source of uncertainty in our simulations, we focus on that topic.

[4] In general, many processes that control ice initiation in clouds remain poorly understood [e.g., Cantrell and Heymsfield, 2005], and historically there have been particularly great discrepancies between theory and measurements in clouds warmer than about  $-15^{\circ}\text{C}$ , where observations have often indicated much more ice than known sources could generate [e.g., Hobbs, 1969; Beard, 1992]. Since the liquid in such clouds never approaches the temperature at which pure water drops begin to freeze at substantial rates (about  $-36^{\circ}\text{C}$  for  $100\text{-}\mu\text{m}$ -diameter drops [Pruppacher and Klett, 1997]), homogeneous drop freezing can be ruled out as an ice source. Homogeneous freezing of the most common aerosol electrolyte solutions, which occurs at even lower temperatures, can also be ruled out [e.g., Koop *et al.*, 2000; Kärcher and Koop, 2005]. With respect to the possible roles of aerosol impurities in promoting ice formation at warmer temperatures, often collectively referred to as heterogeneous ice nucleation mechanisms, it has long been found that measured ice crystal number concentrations often exceed measured ice nucleus number concentrations by orders of magnitude [Mossop, 1970, 1985; Beard, 1992, and references therein], even when ground-based measurements are made in order to definitively rule out errors associated with aircraft measurements [e.g., Mossop *et al.*, 1968]. However, because of the variety of ways in which aerosol impurities can induce freezing, including “contact nucleation” of ice at a drop surface by an impinging ice nucleating aerosol, “deposition nucleation” of ice directly upon an aerosol surface, “condensation nucleation” of ice during drop activation at supercooled temperatures, and “immersion nucleation” of ice in a nucleus-containing drop that later becomes sufficiently supercooled, no single measurement technique exists to fully characterize the ice nucleating ability of an aerosol population [Rogers *et al.*, 2001b], and hope has therefore remained that improved measurements will resolve this discrepancy [Pruppacher and Klett, 1997].

[5] Meanwhile, in the search for other sources of the ice observed in such clouds, numerous laboratory experiments have been carried out to evaluate hypothesized physical mechanisms that could take the small amounts of ice that could be initiated by measured ice nuclei and “multiply” them sufficiently to explain the larger observed ice populations [e.g., Mossop, 1970, 1985; Pruppacher and Klett, 1997]. The only multiplication mechanism that is now included in most microphysically detailed cloud models is the process of ice splinter ejection during riming [Hallett and Mossop, 1974; Mossop and Hallett, 1974], which may produce on the order of one ice crystal per 250 collected drops larger than  $25\ \mu\text{m}$  in diameter and may multiply preexisting ice numbers by at least several orders of

magnitude [e.g., Pruppacher and Klett, 1997], but which appears to be narrowly limited to rime surface temperatures of about  $-3$  to  $-8^{\circ}\text{C}$  [Heymsfield and Mossop, 1984]. However, several additional mechanisms have also been quantified. The shattering of drops as they freeze in free fall has been the subject of many studies, which have converged on the general consensus that as many as about 10% of drops larger than  $50\ \mu\text{m}$  in diameter may shatter in the temperature range  $-5$  to  $-15^{\circ}\text{C}$  into as many as about 15 ice fragments apiece [e.g., Brownscombe and Thorndike, 1968; Hobbs and Alkezweeny, 1968], multiplying total resulting ice by a factor of about two [Pruppacher and Klett, 1997, and references therein]. Fewer studies have examined the production of fragments from ice-ice collisions [Vardiman, 1978; Takahashi *et al.*, 1995], the breakup of ice crystals during sublimation [Oraltay and Hallett, 1989; Bacon *et al.*, 1998], and the shedding of mixed-phase particles during melting [Oraltay and Hallett, 2005]. Of the latter group of processes that are not generally included in cloud models, shattering of drops as they freeze in free fall and fragmentation during ice-ice collisions have been hypothesized to be responsible for the high ice concentrations that have previously been observed in Arctic stratocumulus that are too cold for splinter formation during riming [Rangno and Hobbs, 2001], such as those encountered during M-PACE.

[6] The study that we present here builds upon a body of literature that remains meager in part because of a paucity of field experiments during the Arctic transition seasons, when mixed-phase low-level clouds are ubiquitous [e.g., Shupe *et al.*, 2006]. The two major transition season campaigns prior to M-PACE have been the Beaufort Arctic Storms Experiment (BASE) [Curry *et al.*, 1997], conducted during the autumn of 1984, and the First ISCCP Regional Experiment—Arctic Cloud Experiment/Surface Heat Budget in the Arctic (FIRE-ACE/SHEBA) Program [Curry *et al.*, 2000; Curry, 2001], conducted during the spring of 1998. In simulating observed mixed-phase conditions during both BASE and FIRE-ACE/SHEBA, the most detailed modeling studies to date have been focused primarily on the challenge of maintaining steady ice mass production without fully depleting cloud liquid [Jiang *et al.*, 2000; Morrison *et al.*, 2005, cf. Figures 3 and 1]. This problem has also been identified from a more theoretical standpoint [Harrington *et al.*, 1999; Olsson and Harrington, 2000; Harrington and Olsson, 2001]. A general feature of the foregoing modeling studies is that when ice nuclei are treated diagnostically, without depletion, it is difficult to sustain liquid water in the presence of the ice that is continually produced [e.g., Jiang *et al.*, 2000]. However, when the ice nuclei are treated prognostically, accounting for expected consumption, it can be difficult to sustain steady concentrations of ice because ice nuclei are rapidly depleted without sufficient replenishment [e.g., Harrington and Olsson 2001]. More recently, in a study using M-PACE observations, Prenni *et al.* [2007] conclude that ice nuclei must be treated prognostically in order to maintain liquid water even when ice nucleus concentrations reach very low Arctic values. However, lack of data over the wide ice nucleation parameter space, e.g., mode of nucleation (such as contact or immersion), temperature and supersaturation dependence of each mode, and whether members of the ice nucleus population can act in

one or more modes, has left modeling studies (including this one) with a wide range of tunable parameters that remain underconstrained.

[7] Most other microphysical data gathered within the last few decades in mixed-phase stratocumulus derive from single-aircraft studies in the Arctic and other regions [e.g., Mossop *et al.*, 1972; Hobbs and Rangno, 1985, 1998] that, while less complete for detailed modeling studies, provide much-needed additional statistics. The main pattern found across these studies is a strong correlation between the number of drops larger than about 20  $\mu\text{m}$  in diameter and the occurrence of ice crystal concentrations in excess of observed ice nucleus concentrations in clouds colder than about  $-6^\circ\text{C}$ , a pattern in line with observations obtained during FIRE-ACE/SHEBA [Rangno and Hobbs, 2001]. The main hypothesis that has been advanced to explain this pattern is preferential freezing of some fraction of large drops, perhaps via contact nucleation [Hobbs and Rangno, 1985]. However, Beard [1992] has argued that the required concentrations of contact nuclei are several orders of magnitude higher than observed. Rangno and Hobbs [2001] later hypothesized that ice fragmentation during drop freezing and ice collisions could be multiplication mechanisms that would be enhanced in the presence of large drops and could explain the observations, which we have adopted as a starting place for this work. To our knowledge this hypothesis has not been evaluated quantitatively to date, probably at least in part because of the complexity of three-dimensional interaction among turbulent dynamical and mixed-phase microphysical processes in low-level Arctic clouds, which makes quantifying ice sources extremely difficult. Our overall approach here is to use a subset of the results from Part 1 [McFarquhar *et al.*, 2007], representative of typical glaciated conditions, to evaluate large-eddy simulations with size-resolved microphysics. We then use sensitivity tests to assess the strength of possible ice sources. After describing the data (section 2) and our modeling approach (section 3), we present results (section 4) and discussion (section 5).

## 2. Field Measurements

[8] We focus on in situ measurements that were gathered on 10 October during flight 10a of the University of North Dakota Citation aircraft. As the second of four flights that sampled a widespread mixed-phase stratocumulus deck under steady northeasterly flow conditions during 9–12 October (Verlinde *et al.* [2007], where it is referred to as flight 9b), flight 10a provided multiple cloud profiles under typical conditions [McFarquhar *et al.*, 2007]. Throughout the period, cold-air outbreak conditions, with off-ice flow arriving at the northeastern boundary of the Beaufort Sea, gave rise to persistent convective rolls that were roughly aligned with the flow and had diameters of about 10 km by the time they reached the Alaskan coastline. Flight 10a measurements were made primarily along the coast between Oliktok Point and Barrow and over the NSA site at Barrow (Figure 1).

### 2.1. Meteorological Conditions

[9] Analysis of balloon-borne soundings at Barrow and Oliktok Point indicate a relatively stable cloud top height,

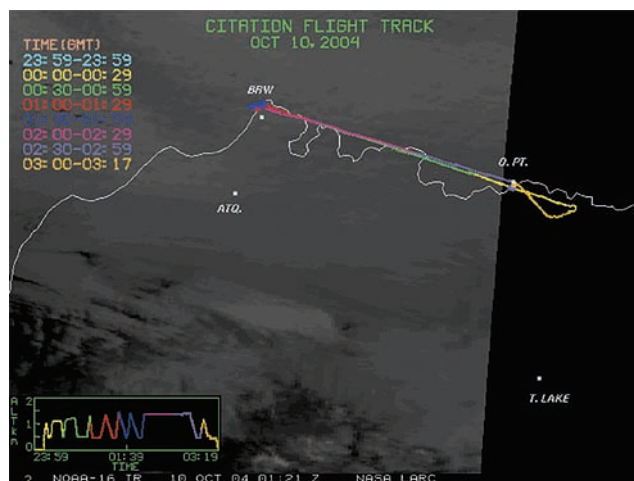


**Figure 1.** Tracks of M-PACE flight 10a between Oliktok Point and Barrow, plotted over infrared AVHRR image, courtesy of Patrick Minnis, NASA Langley.

and cloud top temperatures that fell to about  $-15.5^\circ\text{C}$  by the time of flight 10a (Figure 2). Our objective here is to compare simulation results representative of marine conditions arriving at the coast with data gathered during that flight. We initialize model thermodynamic fields on the basis of a sounding (Figure 3) that was made five hours prior to flight 10a (solid symbol in Figure 2), where adiabatic liquid water content has been added to measured water vapor in the liquid-saturated layer in order to accelerate “spin-up” of the simulations to pseudo-equilibrium. Horizontal winds, which remained steady, are initialized to  $-3 \text{ m s}^{-1}$  zonally and  $-13 \text{ m s}^{-1}$  meridionally. Surface pressure is initialized to 1010.3 mbar. Sea surface temperature is held at  $0.84^\circ\text{C}$ . Surface heat and vapor fluxes are held at 100 and  $120 \text{ W m}^{-2}$  for the first two hours and then derived from similarity theory thereafter, once the momentum deficit in the surface layer has equilibrated. In the absence of downwelling longwave radiative flux measurements at cloud top, the overlying water vapor column is estimated as 2.55 mm in order to induce a downwelling longwave flux of about  $196 \text{ W m}^{-2}$  at model top, chosen to be consistent with estimates of theoretical clear-sky longwave flux at the surface that were derived using a method based on Brutsaert [1975]. Constant profiles of large-scale heat and water vapor advection and subsidence (Figure 3) are specified on the basis of a variational analysis [Xie *et al.*, 2006]. We find that microphysical results are not sensitive to uncertainties in large-scale forcing profiles as long as their combined effect maintains a stable cloud top elevation, as observed.

### 2.2. Cloud Properties

[10] Cloud properties were measured in situ by multiple instruments on the Citation aircraft, as detailed in Part 1 [McFarquhar *et al.*, 2007]. Here we focus on simulating the observed mass, number concentration, and size distribution of liquid and ice during the profiles of flight 10a that were measured nearest to Barrow (Figure 4), as well as size distributions reported from four instruments: a Cloud Particle Imaging Probe (CPI, maximum particle dimension

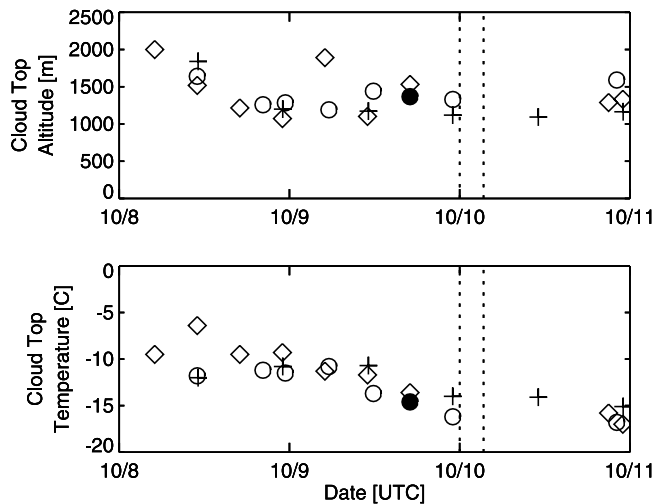


**Figure 2.** Time series of cloud top altitude and cloud top temperature identified from UCAR soundings at Barrow (crosses), M-PACE soundings at Barrow (circles), and M-PACE soundings at Oliktok Point (diamonds). Vertical dotted lines indicate duration of flight 10a. Solid circle indicates profile used to initialize simulations.

>10  $\mu\text{m}$ ), a Forward-Scattering Spectrometer Probe (FSSP, 3–53  $\mu\text{m}$  maximum particle dimension), a one-dimensional cloud probe (1DC, 20–640  $\mu\text{m}$  maximum particle dimension), and a two-dimensional cloud probe (2DC, 125–1060  $\mu\text{m}$  maximum particle dimension, neglecting all smaller sizes owing to possible lack of sensitivity [Strapp et al., 2001]). With the exception of CPI data, for which averaging time varied up to several minutes, all

measurements shown here represent 30-s averages. As discussed in Part 1, owing to the difficulties with FSSP measurements in the presence of ice particles [e.g., Gayet et al., 1996; Field et al., 2003], here we consider measured ice crystal number concentrations only for maximum particle dimensions larger than 53  $\mu\text{m}$  (see section 4.1), and we plot size distributions only when both liquid, mixed-phase and ice measurements are shown side-by-side (see section 4.3). Since airborne 2DC probes may also be subject to errors associated with ice crystal shattering that could lead to overcounting by up to a factor of four [Field et al., 2006], we estimate the possible error in ice number concentration at maximum diameter larger than 53  $\mu\text{m}$  as being at most about half of an order of magnitude. CPI data may further be subject to oversizing of particles, distorting size distribution shape significantly below about 40  $\mu\text{m}$ , depending upon the specific instrument configuration [Connolly et al., 2007]. CPI measurements are not used to estimate number concentration here, but such factors could contribute to explaining the discrepancies between (1) the size distributions measured by the CPI and (2) the more similar features of those measured by the FSSP and predicted by the model (see section 4.3). A modified version of the *McFarquhar and Cober* [2004] phase algorithm, based on *Cober et al.* [2001], was used to identify the phase of each 30-s flight interval as either ice, liquid, or mixed-phase, where mixed-phase indicates that both ice and liquid were detected in the same 30-s interval. Data used by the algorithm include magnitude of voltage change observed by a Rosemount icing detector, visual inspection of particles imaged from the 2DC and CPI, and the shape of the FSSP size distribution, as detailed in Part 1 [McFarquhar et al., 2007].

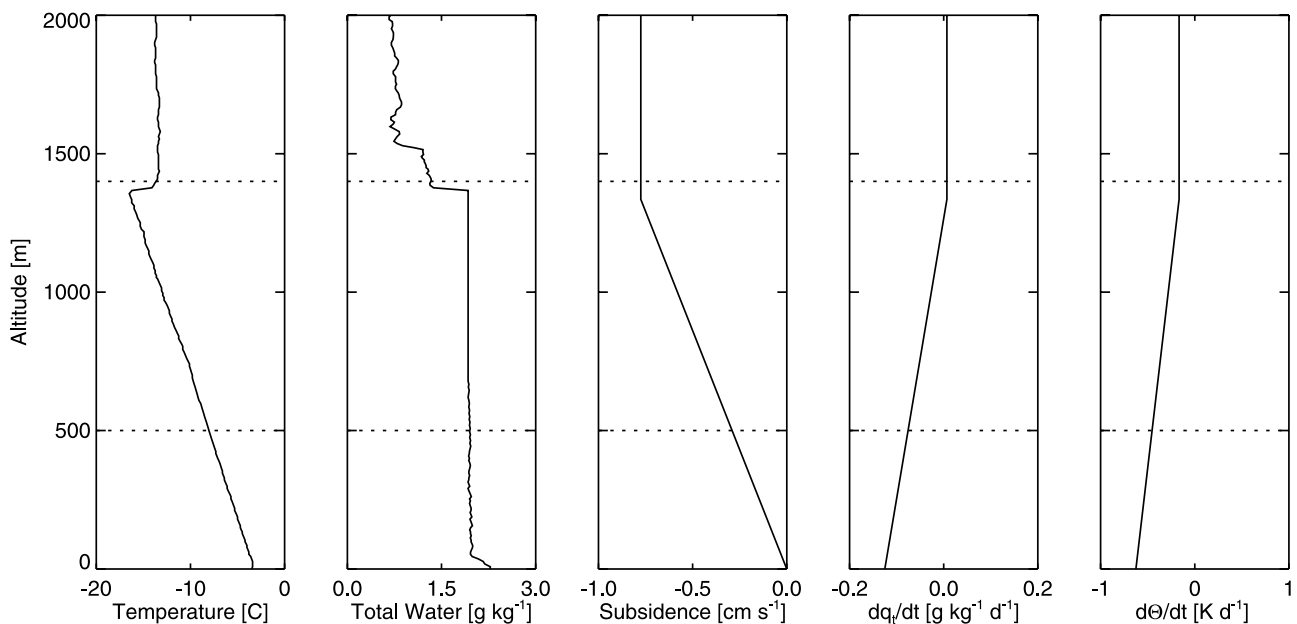


**Figure 3.** Profiles used to initialize and drive M-PACE simulations: temperature and estimated total water (measured water vapor plus adiabatic liquid water content), large-scale subsidence, and large-scale horizontal flux divergences of total water mixing ratio and potential temperature (solid lines). Also shown is typical predicted liquid cloud extent (dotted lines). Sounding measurements correspond to the solid circle in Figure 2. Further details provided in section 2.1.

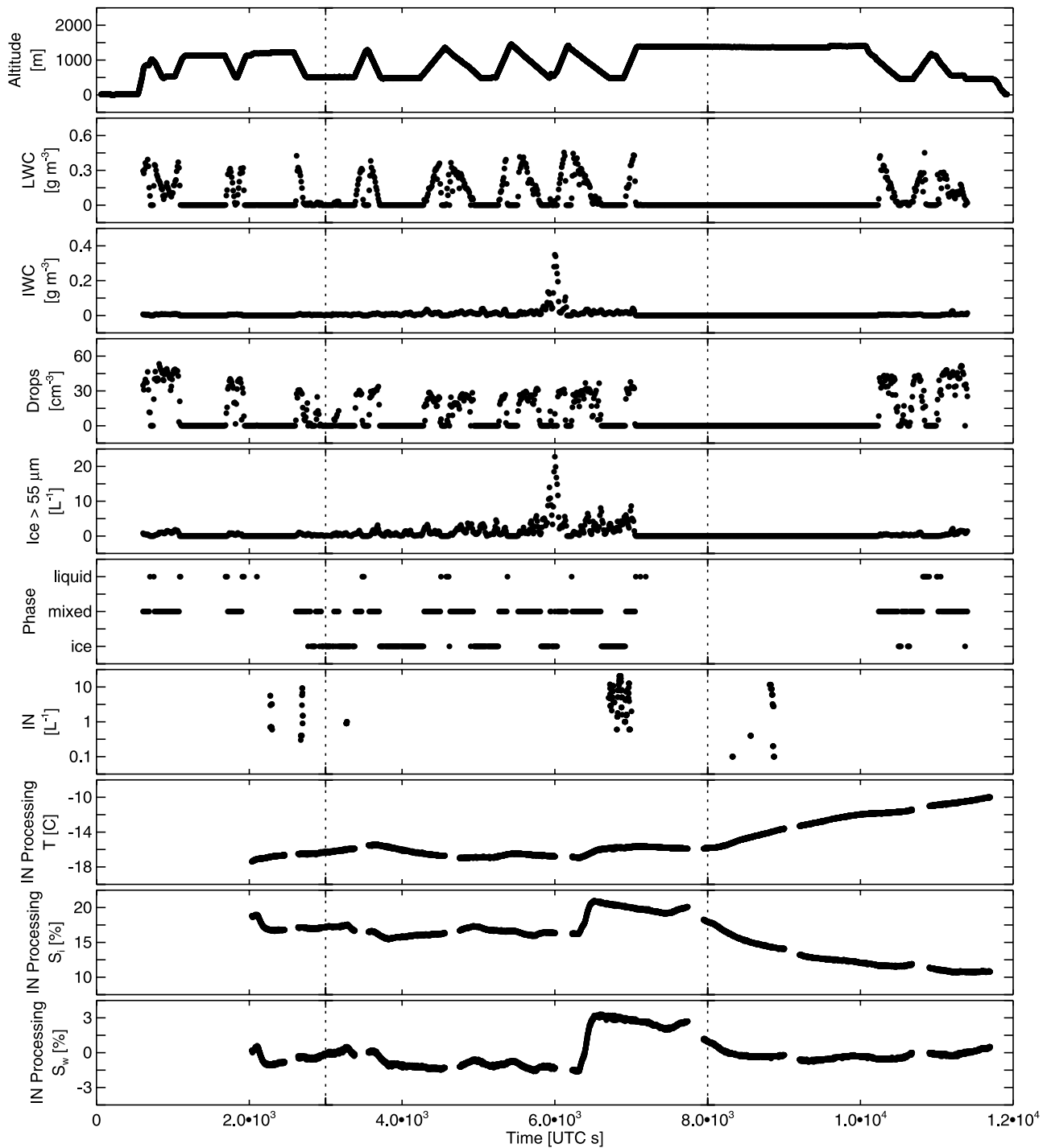


**Figure 4.** Time series of in situ measurements during M-PACE flight 10a (see section 2): aircraft altitude, liquid and ice water content, drop concentration, ice crystal concentration with maximum dimension larger than 53  $\mu\text{m}$ , condensate phase, ice nucleus (IN) concentration when above the detection limit, and IN processing temperature and supersaturations with respect to ice and water. Dotted lines indicate range of data nearest to Barrow that is considered in this study.

### 2.3. Aerosol Properties

[11] In the absence of condensation nuclei data from the Citation aircraft owing to instrument malfunction, dry aerosol size distribution parameters were derived from more limited measurements made on 10 October with a Hand-Held Particle Counter (HHPC) on the Aerosonde unmanned

aircraft and a condensation nuclei counter operated at Barrow by the NOAA Climate Monitoring and Diagnostics Laboratory. The combined number and large-aerosol size distribution measurements were closely matched by a bimodal size distribution with geometric mean diameters of 0.052 and 1.3  $\mu\text{m}$ , standard deviations of 2.04 and 2.5, and

number concentrations of 72 and 2 cm<sup>-3</sup>, respectively (H. Morrison, personal communication, 2006).

[12] In the absence of aerosol composition information, we assume dry aerosol mass to be pure ammonium bisulfate for the purposes of drop activation calculations, consistent with previous observations that indicate a general lack of full neutralization of sulfate aerosols over remote Arctic marine regions [Fridlind *et al.*, 2000]. While preserving the relative aerosol number concentration in each mode, we also reduce the total to 50 cm<sup>-3</sup>, a value that yields the observed cloud droplet number concentrations in the range of 30–40 cm<sup>-3</sup> while leaving a significant reservoir of interstitial particles to act as ice nuclei. We justify this on several grounds. First, the available measurements are insufficient to constrain aerosol properties: no composition information is available and spatiotemporal coverage of both number concentration and size distribution are severely limited. Second, observed drop number concentrations were variable (e.g., range seen in Figure 4), indicating the possibility of variability in aerosol conditions that was not captured by such limited measurements. Third, past aerosol composition measurements over the central Arctic ocean have indicated insoluble mass of about 30% that would result in overestimates of drop activation at a given supersaturation of a similar magnitude if fully soluble mass were assumed [Bigg and Leck, 2001; Zhou *et al.*, 2001], consistent with our lowering of total number.

#### 2.4. Ice Nuclei

[13] The fraction of ambient aerosol particles capable of nucleating ice were measured on the Citation with the CFDC instrument (see section 1), typically operating near cloud-top temperatures (see Figure 4), as reported by Prenni *et al.* [2007]. When operated above ice saturation and below liquid water saturation, the CFDC is sensitive to ice formation only in the deposition mode; when operated above liquid water saturation, it is also sensitive to ice formation in the condensation and immersion modes [see Prenni *et al.*, 2007]. Despite the fact that 27% of the measurements during flight 10a were made above liquid water saturation and therefore included aerosol active in all modes except contact, 96% of the measurements remained below the CFDC detection limit of about 0.1 L<sup>-1</sup> (Figure 4). When values below the detection limit were assumed to be zero, the mean concentration encountered during flight 10a was about 0.2 L<sup>-1</sup>, exceeding zero primarily because of a handful of rare encounters with pockets of air containing concentrations that exceeded the detection limit. Aside, we note that all measurements during the previous flight were made above water saturation, but the mean concentration was unchanged at 0.2 L<sup>-1</sup>. Such low ice nucleus concentrations are not inconsistent with previous measurements regionally and seasonally [Fountain and Ohtake, 1985; Bigg, 1996; Bigg and Leck, 2001; Rogers *et al.*, 2001a, and references therein].

[14] Although the CFDC is expected to undercount ice nuclei by an unknown amount owing to exclusion of aerosols larger than 1.5 μm in diameter and lack of sensitivity to contact-mode nucleation, no instrument has yet been devised to measure all nucleation modes and the CFDC is expected to undercount far less than other methods [e.g., Bigg and Leck, 2001; Rogers *et al.*, 2001b]. For the

simulations here, we interpret flight 10a measurements as indicative of a uniform background ice nucleus concentration in all modes on the order of 0.2 L<sup>-1</sup> (with about a factor of two in uncertainty), on the basis of the approximations that contact nuclei (such as dust) are also active (and therefore counted) in one of the other three modes and that ice nuclei larger than 1.5 μm do not comprise a major proportion of the population. Sensitivity of the simulation results to such assumed background ice nucleus concentrations and their activation conditions is investigated further below.

### 3. Model Description

#### 3.1. Dynamics

[15] The Distributed Hydrodynamic Aerosol-Radiation-Microphysics Application (DHARMA) code [Ackerman *et al.*, 2000] aims to resolve as completely as possible the coupling of cloud motions and size-resolved, mixed-phase microphysics. The three-dimensional model domain is made large enough to span several boundary layer eddies, and grid resolution within that domain is then limited by computational capabilities of current parallel computing platforms. DHARMA performance in recent model intercomparison studies has been evaluated for cases of liquid-phase trade cumulus and stratocumulus [Stevens *et al.*, 2001, 2005] and mixed-phase deep convection [Barth *et al.*, 2007].

[16] DHARMA treats atmospheric and cloud dynamics with a large-eddy simulation code [Stevens and Bretherton, 1996; Stevens *et al.*, 2002] that has been modified to include a dynamic subgrid-scale turbulence model, which has proven useful for reproducing the dynamics of boundary layer stratocumulus under strong inversions [Kirkpatrick *et al.*, 2006]. For the simulations shown here, a domain of 3.2 km by 3.2 km horizontally and 2 km deep is divided into a mesh of 64 × 64 × 96, achieving uniform grid spacings of 50 m horizontally and 20 m vertically. The dynamical equations are advanced using a time step of 5 s, which is lowered when a maximum Courant number of 0.8 is exceeded for the flow, generally resulting in about 10% more time steps than a constant time step of 5 s would have produced in a typical simulation of M-PACE conditions. Results are insensitive to doubling of vertical and horizontal resolution and the associated reduction in dynamical time step.

#### 3.2. Basic Microphysics and Radiative Transfer

[17] Embedded within the dynamics code, DHARMA treats aerosol and cloud microphysics and two-stream radiative transfer with the Community Aerosol-Radiation-Microphysics for Atmospheres (CARMA) code [Ackerman *et al.*, 1995; Jensen *et al.*, 1998]. For the simulations shown here, 20 mass bins each are used to resolve aerosols (0.02–2 μm dry diameter), liquid drops (2–2000 μm diameter), and ice crystals (2–5000 μm maximum diameter). Doubling the number of size bins (decreasing the ratio of particle mass in adjacent bins from 3.0 to 1.7 for both liquid and ice categories) results in more peaked drop size distributions and reduced drizzle production, as expected, indicative of reduced numerical diffusion in coagulation calculations, but changes are similar to those associated

with uncertainties in drop-drop and drop-ice collision and coalescence efficiencies and do not lead to major changes in predicted liquid or ice water path.

[18] All particle categories are treated as spheres for all processes, using the respective bulk densities of ammonium bisulfate ( $1.78 \text{ g cm}^{-3}$ ), liquid water ( $1.0 \text{ g cm}^{-3}$ ), and a range of values for ice ( $0.06\text{--}0.9 \text{ g cm}^{-3}$ ) that is derived as the maximum of 0.9 and the density implied by a relation between particle mass,  $m$  [g], and maximum dimension,  $D$  [ $\mu\text{m}$ ], given by  $m = 0.02 D^{2.2}$ , which lies within the range of values found for rimed particle types [Heymsfield and Kajikawa, 1987]. The approximation of ice as spherical is based on the predominance of irregular shapes (many rimed) and scarcity of pristine crystals during M-PACE (see Part 1), consistent with previous characterizations of Arctic ice crystals [Korolev and Isaac, 1999]. Resulting fall speeds are on the order of 1 and  $2 \text{ m s}^{-1}$  for respective ice diameters of 0.5 and 2 mm at surface pressure. Sensitivity of results to assumed ice density is discussed further below.

[19] Within each liquid and ice mass bin, dissolved ammonium bisulfate is tracked in order to estimate solute effects on the particle growth rates. However, aerosols are treated diagnostically in order to avoid the need for aerosol sources, which would be sorely unconstrained by the measurements. The aerosol size distribution available for activation during each time step is assumed equal to the constant initial size distribution minus the existing number of drops in that grid cell, which are progressively subtracted from the largest aerosol bins.

[20] In addition to aerosol activation, standard microphysical processes acting upon and among the particle sizes and types include condensational and depositional growth, evaporation and sublimation, particle sedimentation, and rime splintering [Pruppacher and Klett, 1997]. For these simulations, activation and vapor exchange processes are calculated with a minimum time step of 0.2 s, depending largely on the local dynamical forcing of supersaturation. Gravitational collection and the associated rime splintering are calculated less frequently, using the dynamical time step, owing to their relatively slow rates of occurrence and the high computational expense. Gravitational collection is solved with a mass- and number-conserving implicit algorithm [Jacobson et al., 1994]. We take into account size-varying collision and coalescence efficiencies for water drops [Hall, 1980; Beard and Ochs, 1984]; ice-liquid and ice-ice collision efficiencies are assumed to have the same size dependencies [e.g., Ovtchinnikov et al., 2000], but coalescence is assumed to be 100% efficient for ice-liquid collisions and zero for ice-ice collisions. In this way, ice-ice collection is neglected owing to its negligible impact on simulations at such low ice concentrations and its high computational expense, but sensitivity tests that include fragmentation during ice-ice collisions (described below) are still provided with an estimate of collision rates.

[21] Two-stream radiative transfer is treated by dividing solar and infrared radiation into 26 and 18 respective wavelength bins and using Mie theory to calculate particle scattering and absorption coefficients and an exponential sum formulation to calculate gaseous absorption and emission [Toon et al., 1989]. To maintain computational efficiency without significant loss of accuracy, radiative transfer calculations are updated every 60 s. The effect of

liquid and ice particle radiative heating and cooling on vapor exchange is also calculated [Ackerman et al., 1995], carrying over to important effects on phoretic forces.

### 3.3. Heterogeneous Ice Nucleation and Ice Multiplication Processes

[22] For the simulations presented here, parameterizations have been added for several additional processes: (1) shattering of drops during freezing, (2) fragmentation during ice-ice collisions, and (3) heterogeneous nucleation that includes the impact of local phoretic forces on the scavenging of ice nuclei.

[23] First, drop shattering is represented by transferring a fraction of large drops ( $>50 \mu\text{m}$  in diameter) that are freezing because of contact ice nucleation or collection of a smaller ice fragment (maximum dimension no larger than half that of the falling drop) into enough equal-sized fragments that an overall factor of two increase in the resulting ice number is induced (see section 1). Computational efficiency is achieved by allowing the freezing fraction to vary up to a maximum value of 25%, such that a single ice destination bin can be found to receive the equal-sized fragments of each drop size in a mass-conserving manner, given their total number.

[24] Second, fragmentation due to ice-ice collisions is represented by applying the Vardiman [1978] parameterization, based on observed impaction of natural ice particles with a plate surface. As an upper limit, considered most appropriate for the collisions of rimed plane dendrites or spatial crystals, the number of fragments ejected from each colliding parent is estimated as a factor of four times the square of each particle's momentum change, resulting in up to thirty fragments per parent. As a lower limit, considered more appropriate for graupel-graupel collisions, the factor of four is reduced by one third, resulting in up to ten fragments per parent. Since detailed guidance on fragment size is not available, all fragments are placed in the bin containing ice of  $50\text{-}\mu\text{m}$  maximum dimension.

[25] Third, turning from ice multiplication to ice initiation, ice nuclei acting in the four standard heterogeneous modes (described in section 1) are represented prognostically as an array of ten elements, ordered from most to least easily nucleated, consumed in any given mode according to ability as a function of temperature and supersaturations with respect to liquid and ice (Table 1 and Appendix A). The underlying assumption of this treatment is that all ice nuclei are capable of acting in any given mode if the appropriate conditions are met, and that nuclei most easily activated in one mode are also the most easily activated in other modes. Any mode can therefore potentially consume nuclei in a given grid cell and time step.

[26] This treatment is based roughly on the properties of an internally mixed aerosol, such as atmospheric dust particles, which are capable of nucleating ice in multiple modes [e.g., Pruppacher and Klett, 1997]. We note that while dust appears to be responsible for the highest local concentrations of ice nuclei observed in the atmosphere to date [DeMott et al., 2003b], it may often account for only about half of typical ice nuclei [e.g., DeMott et al., 2003a]. Measurements have also indicated that about half of Arctic ice nuclei are typically crustal in springtime and that although most remaining ice nuclei are aspherical like dust,

**Table 1.** Ice Formation Mechanisms Included in Model Runs

Mechanism	T, °C	$S^a$	Dependence <sup>b</sup>	Description <sup>c</sup>
<i>Heterogeneous Nucleation</i>				
Contact mode	−4 to −14	−	$f_{in}(T)$	drop + $IN_{aerosol} \rightarrow$ ice crystal
Condensation mode	−8 to −22	$S_w > 0$	$f_{in}(T)$	vapor + $IN_{aerosol} \rightarrow$ ice crystal
Deposition mode	<−10	$S_i > 0$	$f_{exp}(S_i)$	vapor + $IN_{aerosol} \rightarrow$ ice crystal
Immersion mode	−10 to −24	−	$f_{in}(T)$	drop + $IN_{drop} \rightarrow$ ice crystal
<i>Ice Multiplication</i>				
Rime splintering	−3 to −8 <sup>d</sup>	−	$f_{in}(T)$	one ice crystal per 250 collisions
Drop shattering	<0	−	−	$D_{drop} > 50 \mu\text{m}$ , multiplication factor of two
Ice-ice collision	<0	−	−	fragment number based on momentum change
<i>Other Processes</i>				
Ice preactivation	<0	$S_i < 0$	−	evaporated ice residual $\rightarrow IN_{aerosol}$
Evaporation nuclei	<0	$S_w < 0$	−	evaporated drop residual $\rightarrow IN_{aerosol}$
Charge enhancement	<0	−	−	$IN_{aerosol}$ more efficiently scavenged
Evaporation freezing	<0	$S_w < 0$	−	evaporating drop spontaneously freezes
Volume freezing	<0	−	−	spontaneous freezing per unit drop volume
Surface area freezing	<0	−	−	spontaneous freezing per unit drop surface area

<sup>a</sup>Supersaturation with respect to water,  $S_w$ , or ice,  $S_i$ .

<sup>b</sup>Functional dependence takes linear form,  $f_{in}$ , or exponential form,  $f_{exp}$ .

<sup>c</sup>Details provided in section 3 and Appendix A.

<sup>d</sup>Temperature range of rime surface.

they appear to have a different composition [Rogers *et al.*, 2001a]. In the summertime Arctic over ice pack, Bigg and Leck [2001] further identify a correlation of ice nucleus concentration with aerosol concentration in the 50–120 nm size range, and suggest that organic fragments found in the aerosol phase could be the source. With such scant information on noncrystal components, we start here by assuming that all ice nuclei can act in any mode.

[27] Owing to the possible importance of contact nucleation under M-PACE conditions, special attention is paid to the treatment of ice nucleus scavenging rates by drops (see Appendix A). A model such as DHARMA is well suited to provide detailed calculations of ice nucleus scavenging rates since updrafts and downdrafts are represented, and drop surface temperatures as a function of size are also calculated. Scavenging of ice nuclei by existing ice, a removal process that would not cause a phase transformation, is neglected owing to the relative scarcity of ice crystals compared with drop number concentrations. For lack of data, we assume a uniform ice nucleus diameter of  $0.5 \mu\text{m}$  [Rogers *et al.*, 2001a].

[28] An unknown is whether ice nuclei are recycled when ice evaporates before sedimentation loss to the ocean surface. Assuming that all ice particles that evaporate above the surface yield ice nuclei and that those nuclei are also “preactivated” [Roberts and Hallett, 1967; Knopf and Koop, 2006] (most easily activated in each mode) places an upper limit on the possible effect of recycling for several reasons: not all substances may be preactivated [e.g., Mason and Maybank, 1958], dry deposition losses to the ocean surface are neglected, and even ice particles produced from multiplication processes create nuclei in our treatment (since we cannot distinguish them from the ice particles formed by ice nuclei). When this upper limit treatment is implemented (see Appendix A), we find that the initial background ice nuclei are initially sustained in the cloud layer, but simulations return to the same state (after about four hours) that is more quickly reached without recycling:

once the initial background nuclei are cleared from the cloudy boundary layer by the ice particles that do sediment to the surface before evaporating, entrainment again predominates, and recycling is insignificant by comparison. Since boundary layer air likely traveled for about seven hours before reaching Barrow from the point of cloud onset (about 350 km at a mean wind speed of about  $13 \text{ m s}^{-1}$ ), we therefore neglect recycling.

[29] Overall, while our treatment of the standard heterogeneous nucleation modes allows nuclei to be transported and consumed, we do not track the nuclei through possible incorporation into drops during aerosol activation. We instead simply assume that all nuclei are among the unactivated interstitial aerosols when considering contact, condensation, and deposition modes (since drop numbers never exceed about 80% of available aerosol, plenty of aerosols remain everywhere), while conversely assuming that all nuclei are distributed among the drops (more in larger drops) when considering the immersion mode (see Appendix A). We justify this simplified bookkeeping on several grounds. First, tracking a fraction of ice nuclei through activation would require additional information in each liquid and ice mass bin, increasing the total number of variables in each grid cell by almost a third. Second, we have insufficient field data to constrain what fraction of nuclei are soluble. Third, as we demonstrate below, regardless of how easily nuclei are activated in these four standard heterogeneous modes, we find that the total amount of ice nucleated under M-PACE conditions remains at least an order of magnitude below the observed amount by any measure under most assumptions. Thus we consider our treatment appropriately detailed for the simulations presented here.

[30] Out of the foregoing processes that have been added to DHARMA for this study, drop shattering and heterogeneous nucleation (including phoretic scavenging) are included in all runs. The only process treated as a sensitivity test is fragmentation during ice-ice collisions, which gener-

**Table 2.** M-PACE Measurements Versus Simulation Results

Description	LWP, <sup>a</sup> g m <sup>2</sup>	IWP, <sup>a</sup> g m <sup>2</sup>	$N_{ice}$ , <sup>b</sup> cm <sup>-3</sup>
<i>Measurements</i>			
Flight 10a near Barrow	123.4	11.6	–
<i>Model Results</i>			
0.2 L <sup>-1</sup> IN	220.3	0.03	0.00
Slower ice fall speeds	135.6	5.3	0.01
Plus high fragmentation	117.1	6.8	0.05
200 L <sup>-1</sup> IN	163.7	7.1	0.7
Surface source	134.1	10.9	1.9
Evaporation nuclei	137.7	11.9	2.8
Plus electroscavenging	136.0	12.2	3.0
Evaporation freezing	127.8	10.6	2.4
Volume freezing	129.2	11.6	1.9
Surface area freezing	138.0	9.9	1.6

<sup>a</sup>Median of (1) measurements during nine ascents and descents near Barrow (see Figure 4) or (2) model domain-averaged values of path above 400 m calculated at 60-s intervals over hours 8–12 of simulation time (see Figures 5 and 7).

<sup>b</sup>Median of model domain-averaged values of total ice number concentration (in all grid cells containing ice mass mixing ratios exceeding 1 ppm) calculated at 60-s intervals over hours 8–12 of simulation time (no comparable measurement available).

ally has little impact on M-PACE simulations but can lead to “runaway” glaciation during spin-up and under BASE conditions. Uncertainty in the fragmentation parameterization is also considered substantial since it is based on a single field study.

### 3.4. Other Ice Formation Processes

[31] In the absence of sufficient ice formation via the standard four heterogeneous modes and subsequent multiplication (results presented in the following section), four additional formation mechanisms are included in sensitivity tests. First, we consider the possibility that the residuals of a small fraction of evaporating drops become ice nuclei, a hypothesis that has been perhaps most strongly advocated by *Beard* [1992]. Consistent with the preliminary findings of *Rosinski and Morgan* [1991], obtained in a region of Italy that receives both marine and continental air masses, we assume that one in  $10^4$ – $10^5$  evaporating drops creates an ice nucleus in the most easily nucleated class (see Appendix A). We also assume that the nuclei produced are active in all modes as listed in Table 1, except that those in the deposition mode are available at  $-4^\circ\text{C}$  (rather than  $-10^\circ\text{C}$ ), as also suggested by those measurements [*Rosinski and Morgan*, 1991]. Since such nuclei are formed where vapor is unsaturated with respect to liquid but generally remains supersaturated with respect to ice, they may be activated immediately into ice particles, and have therefore been referred to as “transient” [*Rosinski and Morgan*, 1991] or “ephemeral” [*Beard*, 1992]. Since temperatures in the cloudy boundary layer during M-PACE never exceeded  $0^\circ\text{C}$  and recycling of ice nuclei is already neglected (for the reasons described above), there is no additional deactivation to consider, and evaporation nuclei are removed only by consumption.

[32] In the case that evaporation nuclei are not immediately activated into ice, they can dominate total ambient ice nuclei in our simulations, and therefore we have also attempted to account for the increased rate of scavenging

that could occur if the nuclei retain the charges carried by the parent drops [*Beard*, 1992; *Tinsley et al.*, 2000, 2001; *Harrison and Carslaw*, 2003]. In the absence of measurements of particle charge during M-PACE, we estimate a maximum typical value of  $100e$ , with a relatively uniform value throughout the cloud, as suggested by recent measurements in stratocumulus over lake water [*Beard et al.*, 2004]. To roughly account for scavenging enhancement, we adopt a simple estimate based on the calculations of *Tripathi and Harrison* [2002, cf. Figure 4]. We assume that drops smaller than  $36\ \mu\text{m}$  in diameter scavenge the  $0.5\text{-}\mu\text{m}$ -diameter ice nuclei 100 times faster than if they were neutral, drops larger than  $104\ \mu\text{m}$  in diameter scavenge them 10 times faster, and that intermediately sized drops scavenge them at a linearly decreasing rate in between. These multipliers are applied uniformly to the run-time scavenging rates throughout the cloud as an added sensitivity test when evaporation nuclei have already been included.

[33] As a second alternative mode of ice formation suggested in the literature, we consider drop freezing during evaporation, which *Cotton and Field* [2002] found to be their only means of successfully simulating ice formation in wave clouds observed during the 1999 Interaction of Aerosol and Cold Clouds (INTACC) experiment [*Field et al.*, 2001]. When drops shrink to their critical size on the Köhler curve, in addition to subjecting them to a high evaporation rate into the aerosol phase, we also subject them to a freezing rate into the ice phase (in units of  $\text{s}^{-1}$ ) that is chosen to match observations (emulating the ad hoc approach of *Cotton and Field* [2002]). In order to avoid fully depleting cloud liquid during spin-up, the process is turned on only after one hour of simulation time. Whether or not freezing of cloud drops can actually occur in such a manner has not been established experimentally, although hypotheses have been advanced regarding possible physical mechanisms, as we discuss further below (section 5). However, observations have long pointed to a mechanism that could relate ice formation to evaporating drops [e.g., *Hobbs and Rangno*, 1985], and the detailed *Cotton and Field* [2002] modeling study, supported by the extensive INTACC data set, motivates our consideration here.

[34] Lastly, we consider two arbitrary rates of drop freezing throughout the cloud (one rate per unit drop volume and a second rate per unit drop surface area) in order to roughly evaluate the possible role of cloud-phase chemistry in exposing or creating biogenic ice nuclei or surfactant films with ice nucleating properties [e.g., *Leck and Bigg*, 2005; *Zobrist et al.*, 2007]. Like the first two mechanisms described in this section, these merit consideration based on existing literature but could also end up on the long list of previously hypothesized ice formation mechanisms that *Beard* [1992] has described as “weak, inappropriate or nonexistent.”

## 4. Results

[35] All primary runs and sensitivity tests were carried out for twelve hours of simulation time, and results of the last four hours of each such run are summarized in Table 2. Results of secondary sensitivity tests that indicated minimal or negligible effects after four hours were generally not

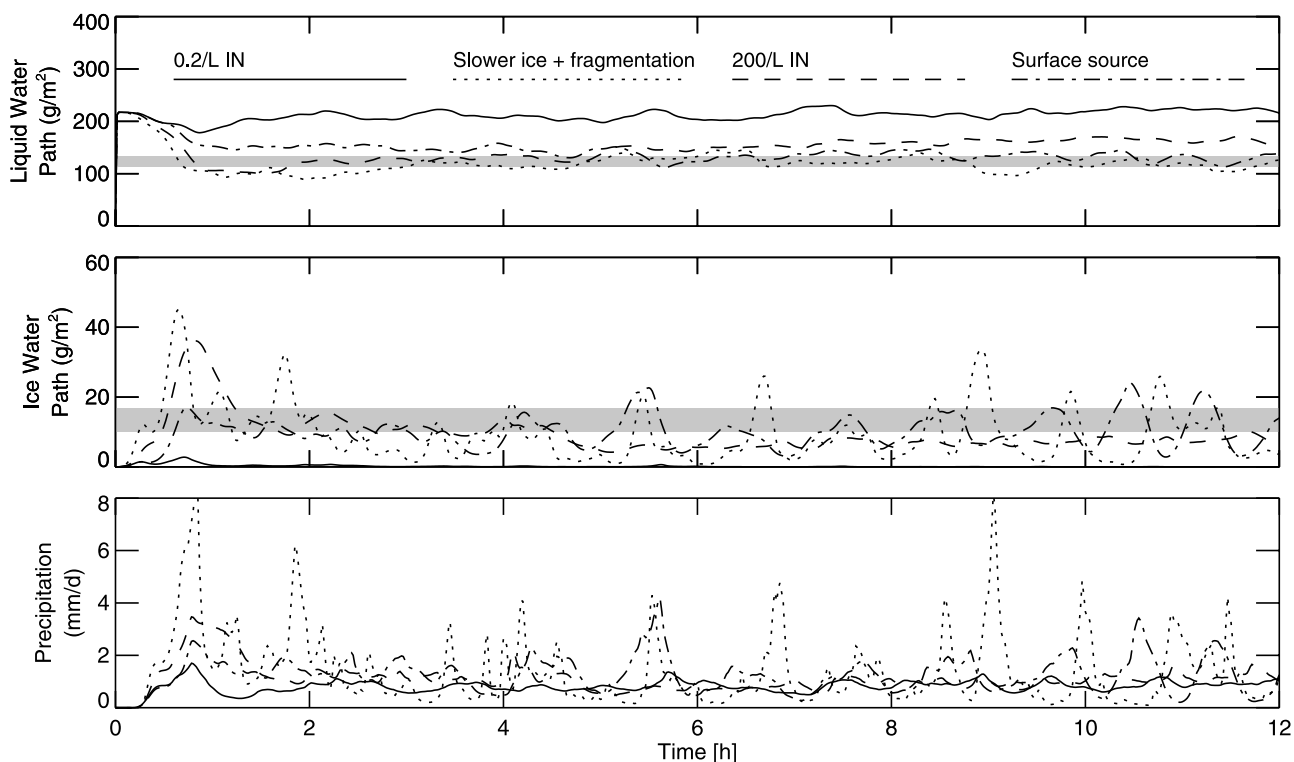


**Figure 5.** Time series of simulated domain-average liquid and ice water path above 400 m and surface precipitation from simulations with 0.2/L ice nuclei (solid line), reduced ice fall speeds and fragmentation (dotted line), 200/L ice nuclei aloft (dashed line), and a surface source of ice nuclei (dash-dotted line). Water paths are compared with the interquartile range derived from in situ measurements above 400 m during M-PACE flight 10a (shaded, see Figure 4). Further details are provided in section 4.1.

completed (owing to computational expense), and are not shown.

#### 4.1. Liquid and Ice Path and Profiles

[36] Simulations initialized and run with observed meteorological conditions (Figure 3), aerosol properties (section 2.3), and ice nuclei (section 2.4), using the baseline estimates of ice density and fall speed (section 3.2) and the standard heterogeneous ice nucleation and ice multiplication mechanisms (rime splintering and drop shattering per section 3.3), produce very little ice during the course of 12-h simulations (Figure 5, solid line, and Table 2). Once initial background ice nuclei are consumed from the boundary layer during the first hour, entrainment provides a negligible source. Simulated ice water path (IWP) then drops to nearly zero and liquid water path (LWP) exceeds the typical range of observations, where observed LWP and IWP are derived by integrating in situ aircraft measurements of liquid water content (LWC) and ice water content (IWC) during all complete flight segments between cloud top and cloud base (about 400 m) near Barrow (see Figure 4).

[37] Consistent with predicted LWP, the profile of simulated LWC also generally exceeds observations, especially at cloud top (Figure 6b versus Figure 6a). These results are independent of the temperature thresholds or individual modes assumed for the heterogeneous ice formation mechanisms listed in Table 1; making all ice nuclei available at cloud base temperatures in all modes or in any given mode provides negligible additional ice (not shown). We also find that ice multiplication mechanisms under these conditions

are weak. Rime splintering is not productive because cloud base temperatures are too low, limiting time-average domain-peak rates to order  $10^{-5} \text{ L}^{-1} \text{ s}^{-1}$ , two orders of magnitude slower than rates typical of a productive rime splintering process [e.g., Beheng, 1987]; the process would need to be active down to particle surface temperatures of about  $-14^\circ\text{C}$  (rather than  $-8^\circ\text{C}$ ) in order to produce significant ice in our simulations. Time-average domain-peak rates of ice production from drop shattering reach typical values of  $10^{-3} \text{ L}^{-1} \text{ s}^{-1}$ , attributable almost entirely to drops frozen by contact nuclei rather than ice fragments, but occurrence is insufficiently widespread to elevate ice concentrations throughout the cloud. Sensitivity tests indicate that concurrent rates of fragmentation from ice-ice collisions at the maximum rate (see section 3.3) are at least three orders of magnitude lower yet, with negligible overall effect (not shown).

[38] As a first sensitivity test, we reduce ice fall speeds sufficiently to increase IWP into the range of observations by lengthening the growth time of the ice particles that are produced. We also activate ice fragmentation at the maximum rate, thereby implementing all possible multiplication mechanisms. When ice density is lowered to a range of  $0.01\text{--}0.9 \text{ g cm}^{-3}$ , fall speeds decrease to about 0.5 and 1  $\text{m s}^{-1}$  for ice diameters of 0.5 and 2 mm at surface pressure (consistent with values found for rimed aggregates, rimed dendrites, or graupel-like snow [Pruppacher and Klett, 1997]), and predicted IWP values cover more of the observed range (Figure 5, dotted line). In this case, results

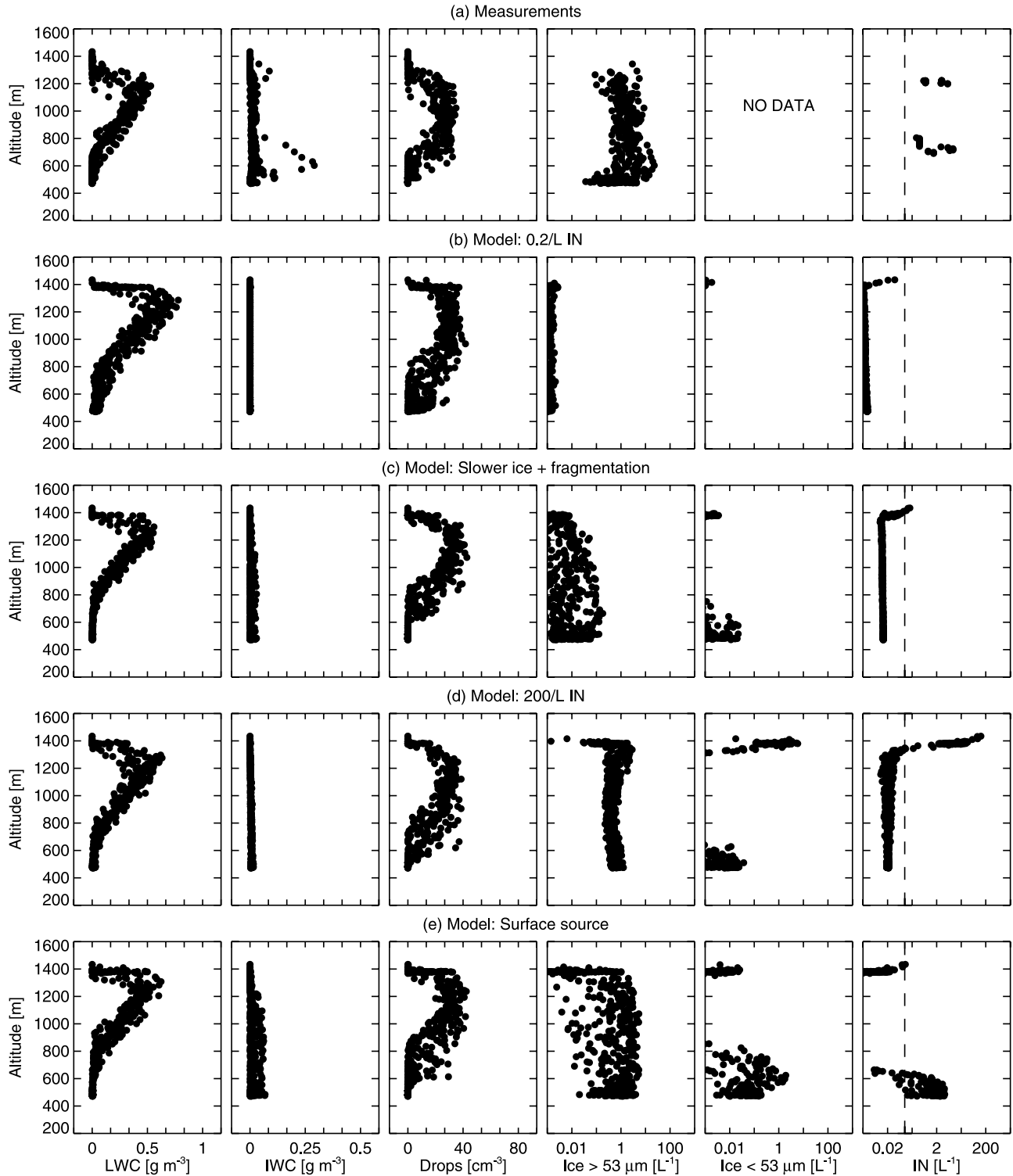


**Figure 6.** M-PACE flight 10a measurements of liquid and ice water content, drops, ice with maximum particle dimension larger and smaller than 53  $\mu\text{m}$  and unactivated ice nuclei (IN) (a) plotted as a function of altitude, compared with simulations with (b) 0.2/L IN, (c) slower ice fall speeds and maximum fragmentation, (d) 200/L IN aloft, and (e) a surface source of IN. A detection limit of  $0.1 \text{ L}^{-1}$  is shown for IN (dashed lines); in-cloud measurements may include activated IN and artifacts (see section 4.2). Model results at 12 h (see Figure 5) are randomly sampled at the altitude of measurements.

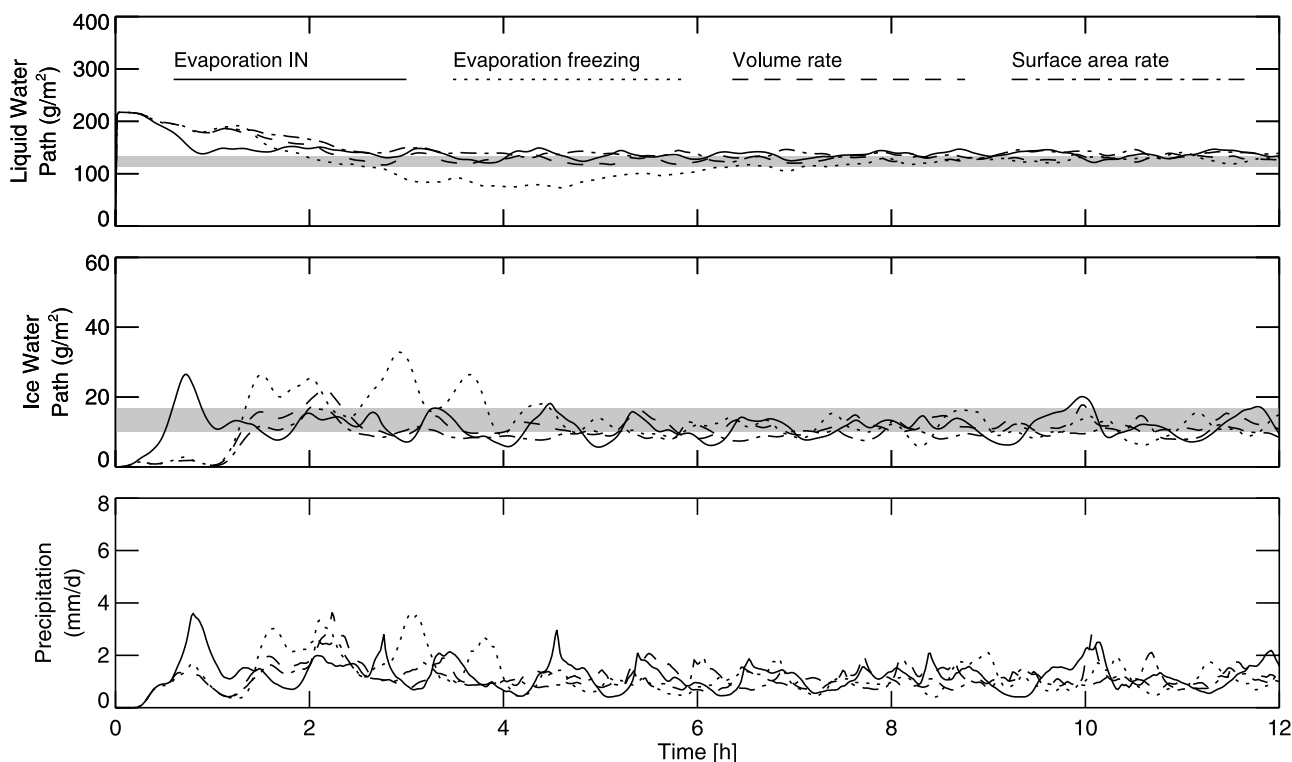


**Figure 7.** Time series of simulated domain-average liquid and ice water path above 400 m and surface precipitation from simulations with ice nucleus formation from residuals of evaporated drops (solid line), freezing during drop evaporation (dotted line), and an assumed freezing rate per unit volume (dashed line) or surface area (dash-dotted line). Water paths are compared with the interquartile range derived from in situ measurements above 400 m during M-PACE flight 10a (shaded, see Figure 4). Further details provided in section 4.1.

appear more consistent with profile measurements, except that simulated ice number concentrations at maximum dimensions larger than  $53 \mu\text{m}$  remain about two orders of magnitude lower than measured (Figure 6c versus Figure 6a). Since ice fall speeds are not well constrained, this result could be realistic if the number of ice is greatly overestimated by the measurements (see section 2.2), as we discuss further below.

[39] For the next two sensitivity tests, we aim to bring predicted IWP into the range of observations by instead increasing ice nucleus concentrations. We first aim to increase ice nuclei sufficiently above the boundary layer, operating on the common baseline assumption that surface fluxes of ice nuclei are negligible by comparison with the background atmospheric reservoir in the Arctic [e.g., Pinto, 1998; Harrington and Olsson, 2001]. Above the boundary layer, we find that three orders of magnitude additional background ice nuclei ( $200 \text{ L}^{-1}$ ) are required to bring IWP into the range of observations (Figure 5, dashed line), and more if the nuclei are assumed to act only in the contact mode (not shown). While predicted ice number concentrations now increase into the range of observations (Figure 6d versus Figure 6a), such high ice nucleus concentrations have rarely been measured aloft in the Arctic or anywhere else [e.g., Pruppacher and Klett, 1997; Rogers et al., 2001a]. Aside, we note that attempting to initiate a liquid cloud in the presence of such high ice nucleus concentrations is difficult; we perform this sensitivity test by raising ice nucleus concentrations only above the boundary layer,

such that ice nuclei are entrained into the domain and steady state can be reached relatively quickly.

[40] When we next instead aim to provide a sufficient surface source of ice nuclei, we assume that they are the most easily nucleated in their class (active at the warmest possible temperature and the lowest possible supersaturation, see Table 1). We find that holding the concentration constant at a minimum value of  $6 \text{ L}^{-1}$  in the surface layer (below 100 m) is required to sustain predicted IWP near the range of observations (Figure 5, dash-dotted line). Since nuclei from the surface source can be efficiently consumed in any mode (because cloud base regions are supercooled and supersaturated with respect to both liquid and ice and scavenging is sufficiently active), these results are remarkably insensitive to whether nuclei are assumed to operate in all modes or any single mode (not shown). Predicted ice number concentrations are again in the range of observations (Figure 6e versus Figure 6a), but even the easily nucleated surface sources elevate ice nucleus concentrations up through cloud base in excess of M-PACE measurements (e.g., Figure 6e versus Figure 6a), as we discuss further in the following section.

[41] In the last four sensitivity tests, our goal is to determine whether any of the alternative ice formation mechanisms described in section 3.4 could be consistent with the M-PACE measurements. Starting with evaporation nuclei, we find that if one in  $5 \times 10^5$  evaporating drops creates an ice nucleus as described in section 3.4, both predicted IWP and LWP remain near the observed ranges

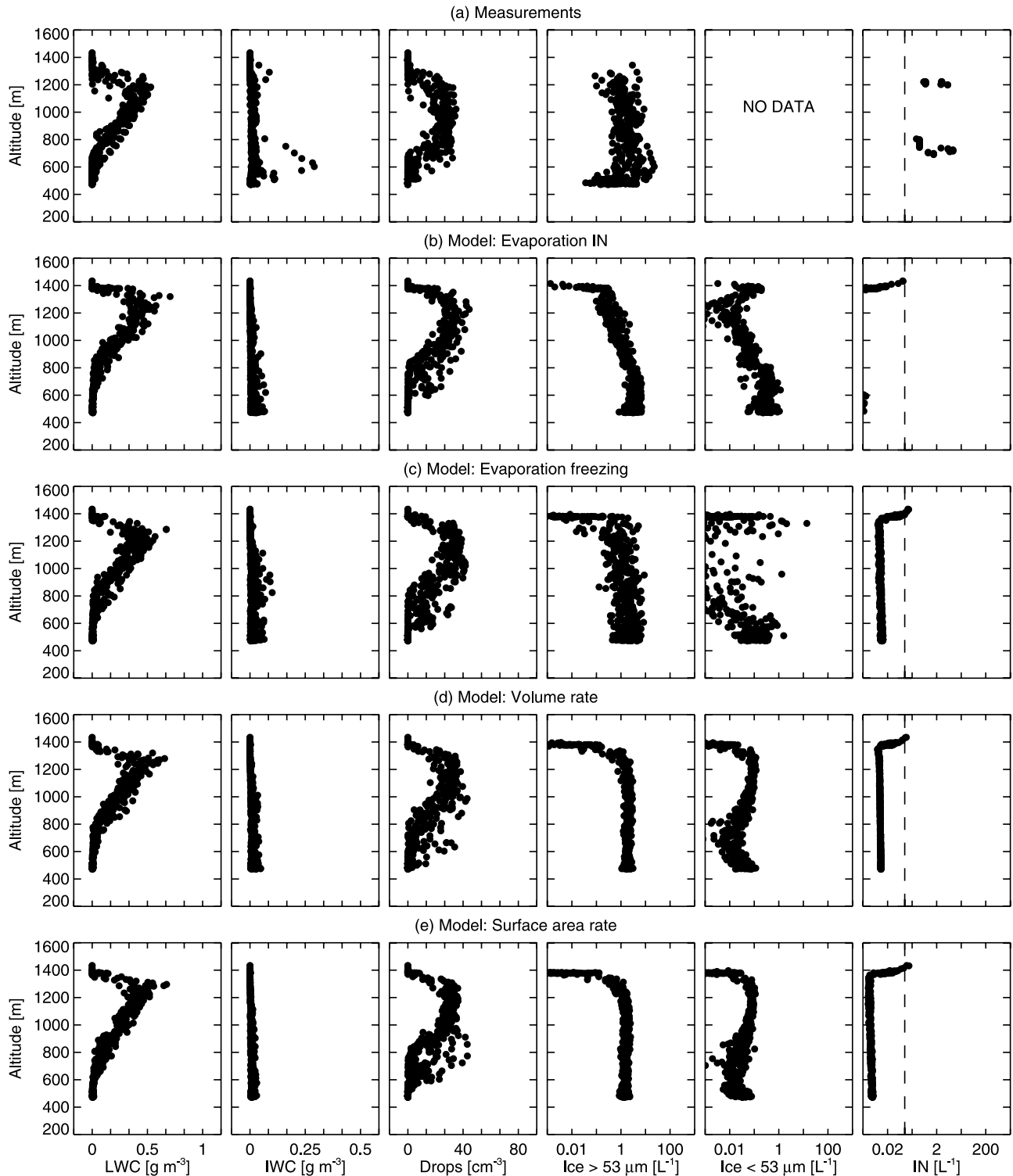


**Figure 8.** M-PACE flight 10a measurements of liquid and ice water content, drops, ice with maximum particle dimension larger and smaller than 53  $\mu\text{m}$  and unactivated ice nuclei (IN) (a) plotted as a function of altitude, compared with simulations with (b) evaporation IN formation, (c) drop freezing during evaporation, and an assumed rate of freezing per unit (d) volume or (e) surface area. A detection limit of  $0.1 \text{ L}^{-1}$  is shown for IN (dashed lines); in-cloud measurements may include activated IN and artifacts (see section 4.2). Model results at 12 h (see Figure 7) are randomly sampled at the altitude of measurements.

(Figure 7, solid line) and profiles of liquid and ice mass and number concentration are also remarkably well reproduced (Figure 8b versus Figure 8a). Adding possible electrical effects to the scavenging treatment increases the predicted ice mass negligibly (see Table 2) because the nuclei produced do not build up sufficiently to be scavenged.

[42] The parameterization for evaporation ice nuclei is straightforward to apply because the rate of ice nucleus formation is bounded by the literature [Rosinski and Morgan, 1991], but when we turn to the remaining three mechanisms, we have no such guidance as to the rates that should be chosen [e.g., Cotton and Field, 2002]. Trial and error is required to find freezing rates that result in simulated IWP values that stay near the observed range (Figure 7, dashed, dotted, and dash-dotted lines). That freezing rate turns out to be about four to five orders of magnitude slower than the rate at which drops would be lost if they were being frozen homogeneously, and is therefore roughly equivalent to freezing one in  $10^4$ – $10^5$  of evaporating drops. It is therefore not surprising that results appear similar to the case of evaporation nuclei (where nuclei are produced at about the same rate), although some differences appear in the range and vertical distribution of resulting ice number concentrations (Figure 8c versus Figure 8b). Adequate freezing rates per unit drop volume or drop surface area (applied to all drops rather than only evaporating drops) turn out to be about  $10 \text{ cm}^{-3} \text{ s}^{-1}$  and  $0.004 \text{ cm}^{-2} \text{ s}^{-1}$ , respectively. The latter is about 2500 times slower than surface film freezing rates measured in the laboratory by Zobrist *et al.* [2007] at midcloud temperatures of  $-13^\circ\text{C}$ , and is therefore roughly equivalent to assuming that one in 2500 drops of all sizes carry such a film. Both freezing rates also generate LWC, IWC, drop, ice, and ice nucleus concentration profiles within the observed ranges (Figures 8d and 8e).

[43] When the parameterization for fragmentation during ice-ice collisions is included as a sensitivity test, operating at the maximum rate (see section 3.3), the effect is strongest when ice fall speeds are slower (see Table 2) and can be considered minor or negligible in all other cases (not shown).

#### 4.2. Ice Nucleus Profiles

[44] It is impossible to get a full picture of the ice nucleus fields during flight 10a because only 4% of 8265 measurements exceeded the CFDC instrument detection limit of about  $0.1 \text{ L}^{-1}$ . Values that were high enough to exceed the detection limit occurred in limited discrete locations during the several-hour flight, primarily in the immediate vicinity of Barrow (see Figures 1 and 4), a pattern evident also in the flight 10a CFDC measurements (not shown), perhaps indicating a local source near Barrow. A handful of the remaining instances of high ice nucleus concentration occurred in cloudy air (e.g., Figures 4 and 6a), where the CFDC may have been measuring nuclei contained in small ice particles (activated nuclei) or may have been influenced by shattering of drops on the inlet. CFDC data from flights before and after flight 10a appear similar in all these aspects. Peak concentrations were low compared with CFDC measurements in springtime during FIRE-ACE/SHEBA over ice [Rogers *et al.*, 2001a], but appear consistent with other measurements in the Arctic during autumn [e.g., Bigg, 1996].

[45] In simulations, predicted unactivated ice nucleus concentrations always fall below the CFDC detection limit in upper in-cloud regions (Figures 6 and 8), generally consistent with observations. When the only ice nucleus source is assumed to be the overlying free troposphere, concentrations below cloud have the same value as within the cloud, consistent with a well-mixed boundary layer (Figure 6d). However, when a surface source is assumed to be present, values below the cloud are greater (Figure 6e); unless the source is assumed to be in the most easily activated class, ice nuclei are also elevated above the detection limit throughout the cloud layer (not shown). Even with a source easily activated in all modes, 69% of the model points in the elevation range 400–600 m are more than twice as high as the CFDC detection limit, whereas only 6% of measurements in that elevation range are above the detection limit (see Figure 6e). Since predicted ice nucleus concentrations fall rapidly in this elevation range and no CFDC measurements were actually made below about 400 m, we do not entirely rule out the possibility of a surface source of easily activated nuclei. However, it appears statistically improbable that a sufficient surface source was present to explain the observations unless they were not detectable by the CFDC (e.g., larger than  $1.5 \mu\text{m}$  in diameter or active only in the contact mode).

[46] In contrast to a source located at the surface or at cloud top, evaporation nuclei produce a volume source concentrated at cloud base in our simulations. Reflecting this, we note that predicted unactivated evaporation nuclei do build up to values that are usually above the CFDC detection limit at cloud base if the evaporation nuclei are active in the deposition mode at a maximum temperature of  $-10^\circ\text{C}$  (not shown) rather than  $-4^\circ\text{C}$  (see section 3.4). There may also be the possibility that such nuclei are not detectable by the CFDC if heating destroys their activity, as reported by Rosinski and Morgan [1991] at temperatures over  $15^\circ\text{C}$ . Since volume and surface drop freezing rates produce ice independent of background nuclei, they create no such unique signatures in predicted ice nucleus profiles (Figures 8d and 8e).

#### 4.3. Liquid and Ice Particle Size Distributions

[47] To compare the cloud particle size distributions predicted in the foregoing simulations with measurements of the CPI, FSSP, 1DC and 2DC (Figures 9 and 10), we take the following approach. First, we consider the averaging time of each measurement. CPI measurements represent segments of flight time of 60 s to several minutes (in order to obtain statistically relevant samples), whereas the remaining instruments represent segments of 30 s. Since typical in-cloud flight speeds were on the order of 50–100 m/s, we take the simplified approach of averaging over one model grid cell (50 m) per second of flight time. Second, we average over randomly sampled model grid cells in the altitude range representative of each measurement in order to roughly capture the distribution of data as a function of altitude (e.g., whether sampling may have been more concentrated at cloud top or bottom). Finally, for the 30-s samples, we also identify the phase of the “model sample”: samples are identified as clear air if they contain less than  $0.001 \text{ g m}^{-3}$  of condensate and otherwise as either liquid phase if they contain less than 10% mass fraction of ice and

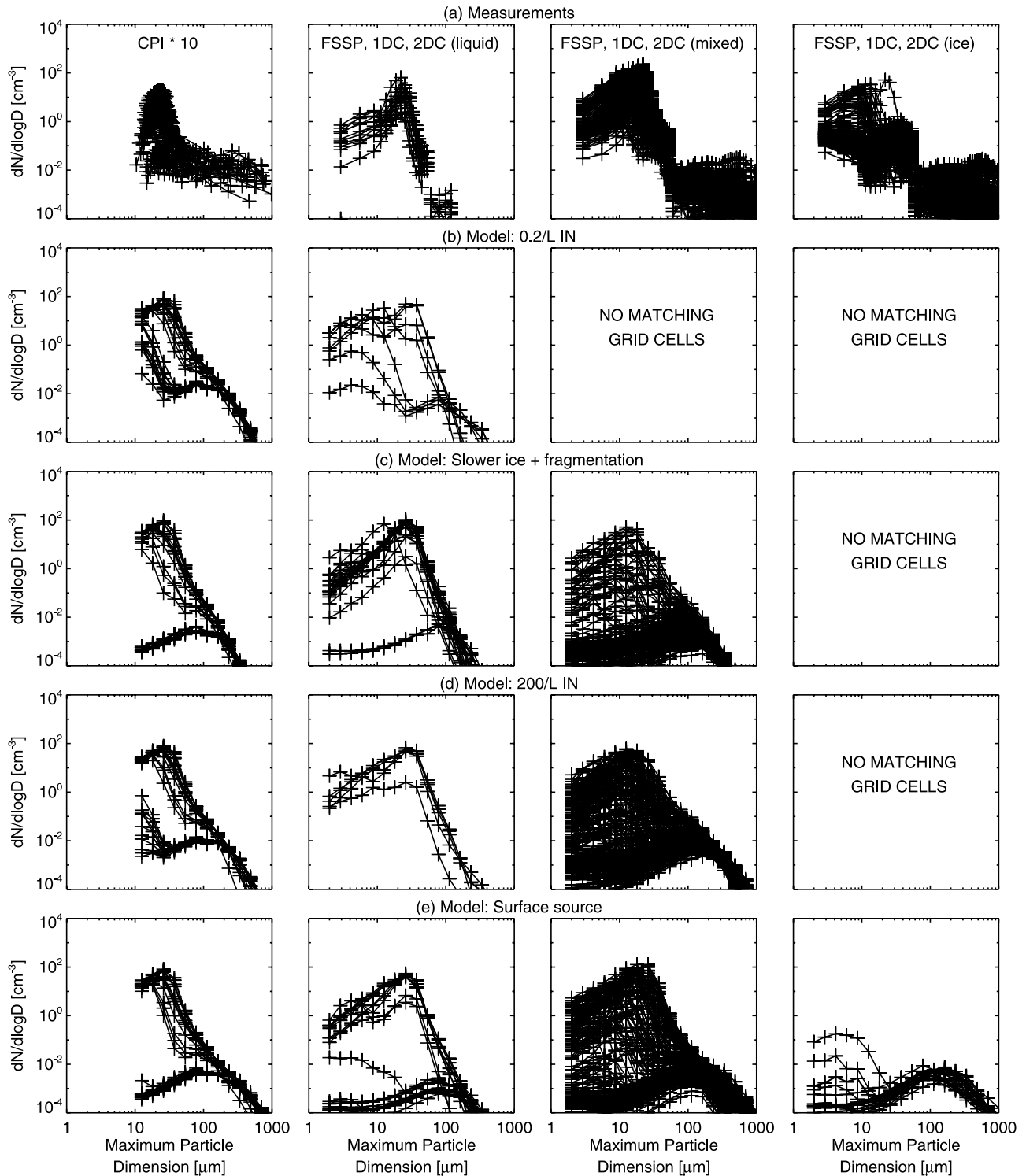


**Figure 9.** (a) M-PACE flight 10a measurements of cloud particle size distribution made by the CPI instrument and by the FSSP, 1DC, and 2DC instruments in ice-free, mixed-phase, and liquid-free regions, compared with (b–e) random samples averaged over the measurement altitude ranges from the same model fields used for Figure 6 (see section 4.3). Size distribution measurements are subject to errors and artifacts (see section 2.2).

fewer than  $0.01 \text{ cm}^{-3}$  particles in the 2DC size range (to avoid significant violations of the phase discrimination described in Part 1), ice phase if they contain less than 10% mass fraction of liquid, or mixed-phase if they contain

at least 10% mass fraction of both liquid and ice. In the case that no randomly selected samples are identified as ice, for instance, no distributions are plotted in that category (no matching grid cells). Aside, we note that while FSSP size

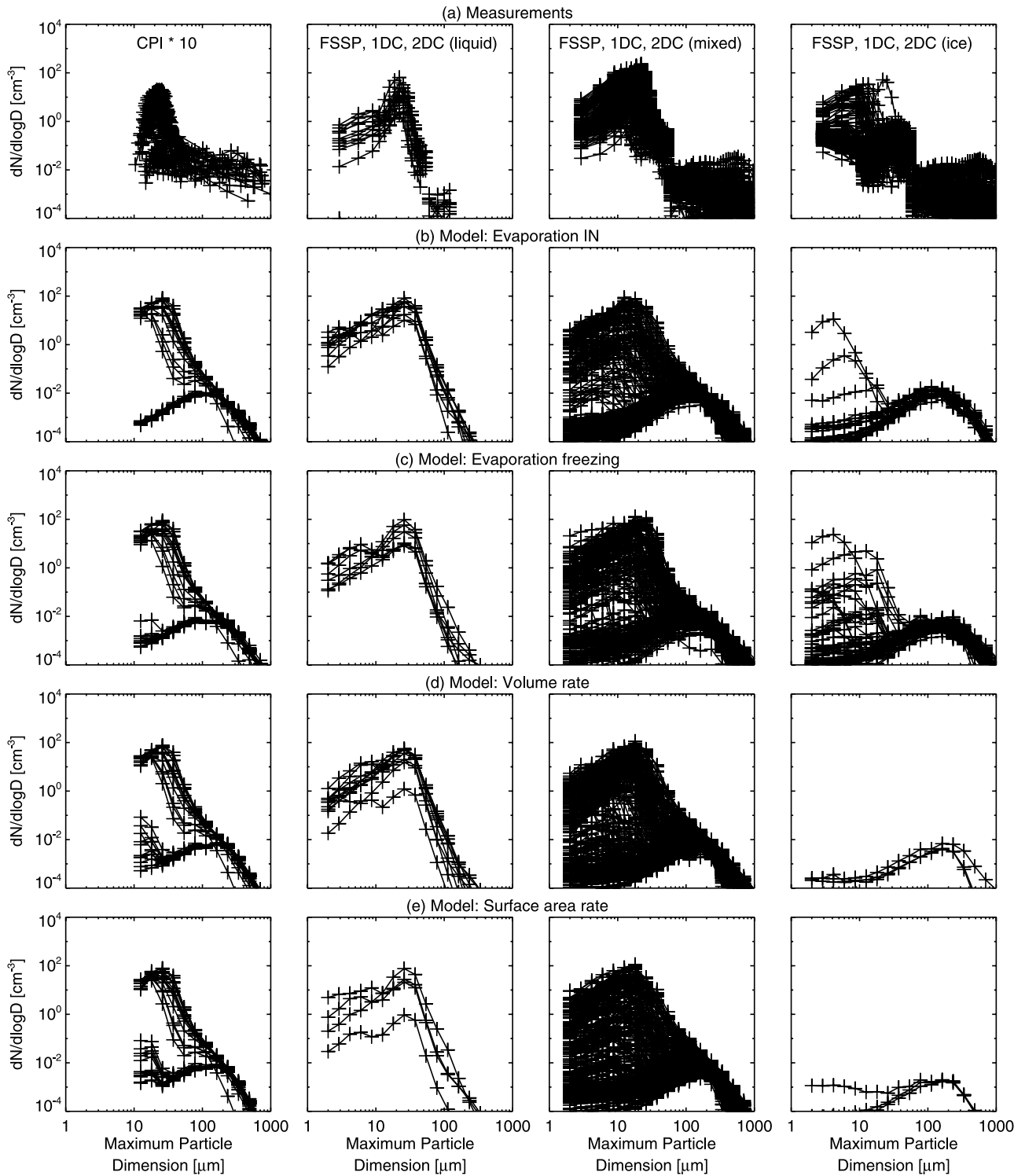


**Figure 10.** (a) M-PACE flight 10a measurements of cloud particle size distribution made by the CPI instrument and by the FSSP, 1DC, and 2DC instruments in ice-free, mixed-phase, and liquid-free regions, compared with (b–e) random samples averaged over the measurement altitude ranges from the same model fields used for Figure 8 (see section 4.3). Size distribution measurements are subject to errors and artifacts (see section 2.2).

distributions are expected to be most accurate in the ice-free cloud regions, we plot them in all cloud phases, remaining cognizant of the errors that can occur in the presence of ice (see section 2.2).

[48] Overall, simulations that most underpredict ice number concentrations (Figure 6) always exhibit lack of sufficient glaciation (Figure 9). Also, glaciation is most extensive when a cloud-base source of ice is present: a

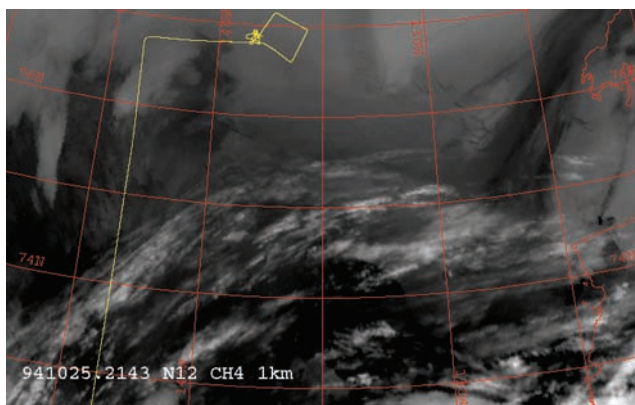


**Figure 11.** Tracks of BASE flight 18A plotted over infrared AVHRR image, courtesy of Marion Legg, Bay Area Environmental Research Institute.

sufficient surface source, evaporation ice nuclei, or evaporation freezing (Figures 9 and 10). When drop freezing rates per unit volume or per unit surface area are tuned to achieve the measured IWP, results lie somewhere in between; glaciation occurs, but is notably insufficient (Figure 10). Since chemistry could occur in localized regions or any number of ways not captured by our simple fitting of freezing rates, these results are interesting and noteworthy. However, from the standpoint of comparing simulations with all available measurements, because a surface source appears likely to be inconsistent with the ice nucleus measurements, we conclude that evaporation nuclei or evaporation freezing provide the best overall agreement thus far.

#### 4.4. Simulations of BASE Case 18

[49] To further probe the two mechanisms that performed best under M-PACE conditions, we briefly examine flight 18A from the BASE campaign (Figure 11), the only transition season case of observed mixed-phase low-level cloud that to our knowledge has already been studied using eddy-resolving simulations [Jiang *et al.*, 2000]. This case provides a strong contrast in dynamical conditions, with a wispy cloud forming in a layer decoupled from the surface, where heat fluxes are near zero over the ice pack [Pinto and Curry, 2001]. We derive an initial sounding from archived aircraft observations and estimate large-scale forcings from National Center for Environmental Prediction (NCEP) re-analysis fields (Figure 12). Model domain and grid parameters are unchanged from those described above. In the absence of ice nucleus measurements, we assume a uniform M-PACE value of  $0.2 \text{ L}^{-1}$ . In the absence of aerosol size distribution measurements, we use the M-PACE size distribution parameters. In the absence of drop concentration measurements for flight 18A [Pinto, 1998; Pinto and Curry, 2001], we assume aerosol numbers that achieve peak drop concentrations similar to the experiment-wide mean of  $47 \text{ cm}^{-3}$  [Pinto and Curry, 2001], conditions also similar to M-PACE flight 10a. In the absence of data on ice crystal habit, considering the likelihood of considerably less riming than during M-PACE owing to at least five times less liquid water path, we initially choose the slower fall speeds that were used as a sensitivity test during M-PACE.

[50] With  $0.2 \text{ L}^{-1}$  ice nuclei and standard ice formation and multiplication mechanisms operating, simulated LWP builds monotonically, quickly exceeding observations (Figure 13, solid line). Since many parameters are poorly constrained, we consider a number of sensitivity tests (only one shown). We find that results are insensitive to further slowing ice fall speeds, increasing drop number, or recy-

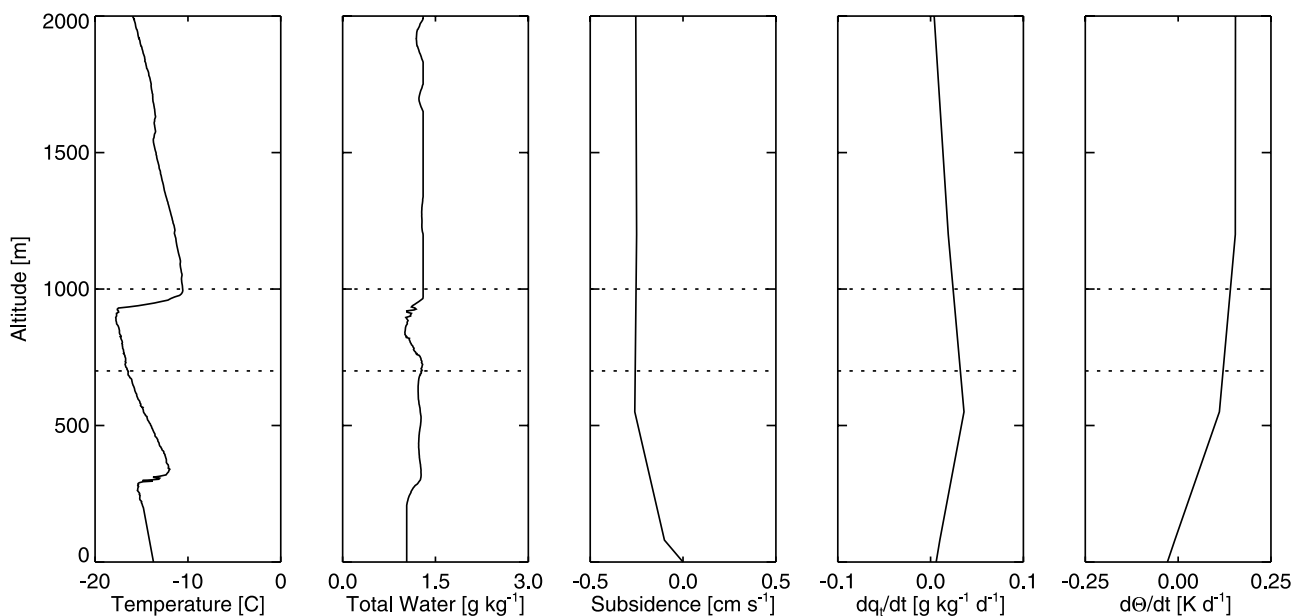


**Figure 12.** Profiles used to initialize and drive BASE simulations: temperature and estimated total water (measured water vapor plus adiabatic liquid water content), large-scale subsidence, and large-scale horizontal flux divergences of total water mixing ratio and potential temperature (solid lines). Also shown is typical predicted liquid cloud extent (dotted lines). Further details provided in section 4.4.

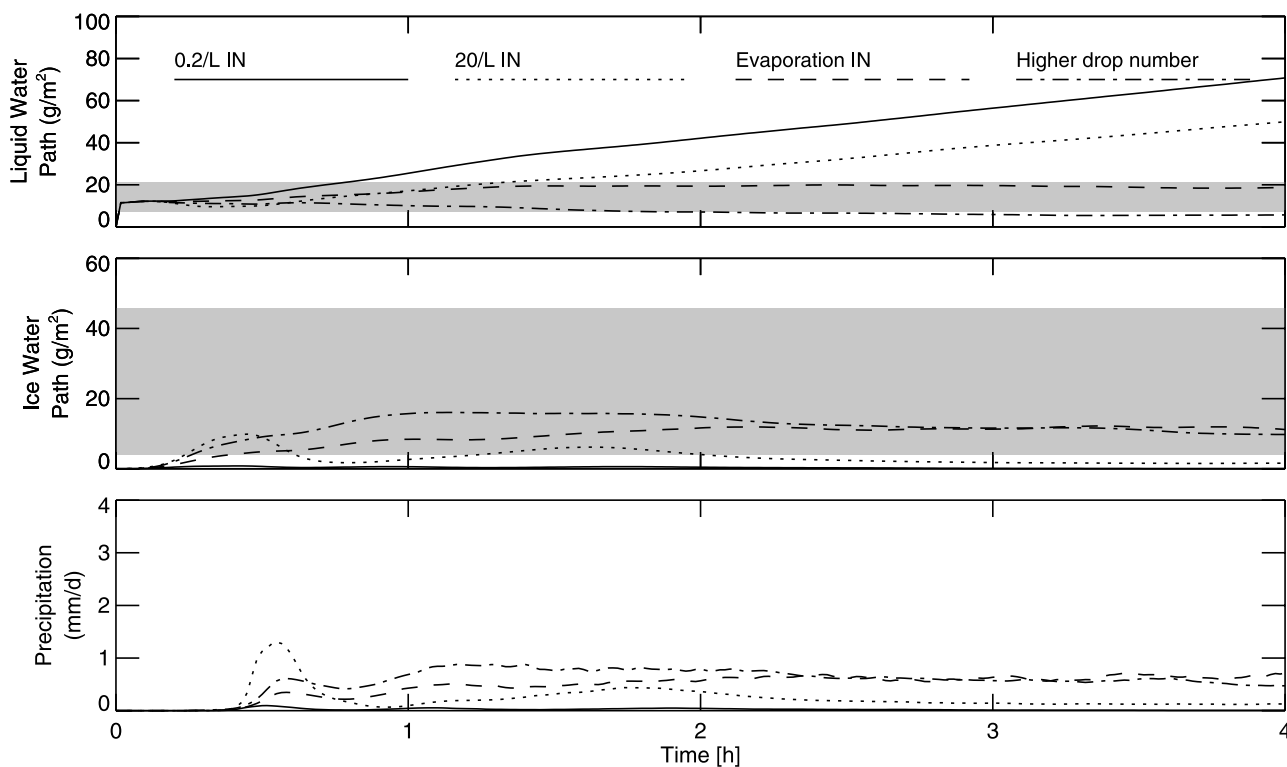


**Figure 13.** Time series of simulated domain-average liquid and ice water path and surface precipitation from simulations with 0.2/L ice nuclei (solid line), ice nuclei elevated to 20/L aloft (dotted line), evaporation nuclei (dashed line), and evaporation nuclei with increased drop number concentration (dash-dotted line), compared with the range derived from in situ observations during BASE flight 18A and the case 18 statistics presented by *Pinto and Curry* [2001] (shaded). Further details provided in section 4.4.

cling ice nuclei; they are only sensitive to decreasing drop number substantially or increasing ice nuclei aloft substantially, which both limit LWP growth (e.g., Figure 13, dotted line) and the ability to sustain significant ice, and therefore appear unlikely. We do not consider a surface source of ice nuclei here owing to the decoupled boundary layer conditions and the short simulation time; such a source cannot be ruled out despite the expected autumn season scarcity of nuclei [*Bigg, 1996; Rogers et al., 2001a*].

[51] When evaporation nuclei are added, formed by one in  $10^4$  evaporating drops (twice the rate required for the M-PACE simulations, but within the range suggested by literature), the simulated LWP and IWP equilibrate in the range of observations (Figure 13, dashed line). If ice fall speed is reduced or drop number increased, predicted LWP is reduced, but still equilibrates near the observed range (Figure 13, dash-dotted line). However, when ice fragmentation is included at the maximum rate as a sensitivity test, the cloud experiences “runaway” glaciation; when the rate is reduced by one third, there is a modest impact on glaciation, and equilibration is achieved at a slightly lower LWP value (not shown). Overall, we find that, although this case is not well constrained by measurements and there is greater uncertainty regarding the role of ice-ice collisions, it is nonetheless straightforward to replicate available measurements using the evaporation nuclei mechanism under a wide range of assumptions.

[52] Turning next to the evaporation freezing mechanism, when implemented using the same rate as during M-PACE,

cloud liquid water is fully consumed and the cloud disappears (Figure 14, solid line). When the freezing rate is reduced sufficiently (by a factor of five), LWP stabilizes, but at a level that exceeds measurements by a factor of about two (Figure 14, dotted line). If ice density is then reduced by a factor of two, all liquid water is again rapidly consumed (Figure 14, dashed line). If the lowest ice density is retained, but freezing rate is again lowered (by another factor of two), LWP again stabilizes, but still at a high value (Figure 14, dash-dotted line). The evaporation freezing mechanism, in summary, is more prone to unstable results. Since this case study is so poorly constrained, we do not consider further efforts worthwhile. However, this brief modeling survey, using the limited additional field data available at this time, demonstrates that the evaporation nucleation mechanism may produce stable mixed-phase clouds under a wider range of conditions than the evaporation freezing mechanism, at least in the manner that we have implemented each.

[53] Profiles of LWP, IWP, drop and ice number, and ice nucleus concentration compared among several runs and with the available measurements are also shown in Figure 15, for completeness.

#### 4.5. Summary

[54] The foregoing results can be briefly summarized as follows:

[55] 1. In simulations of mixed-phase stratocumulus forming under M-PACE meteorological and aerosol con-

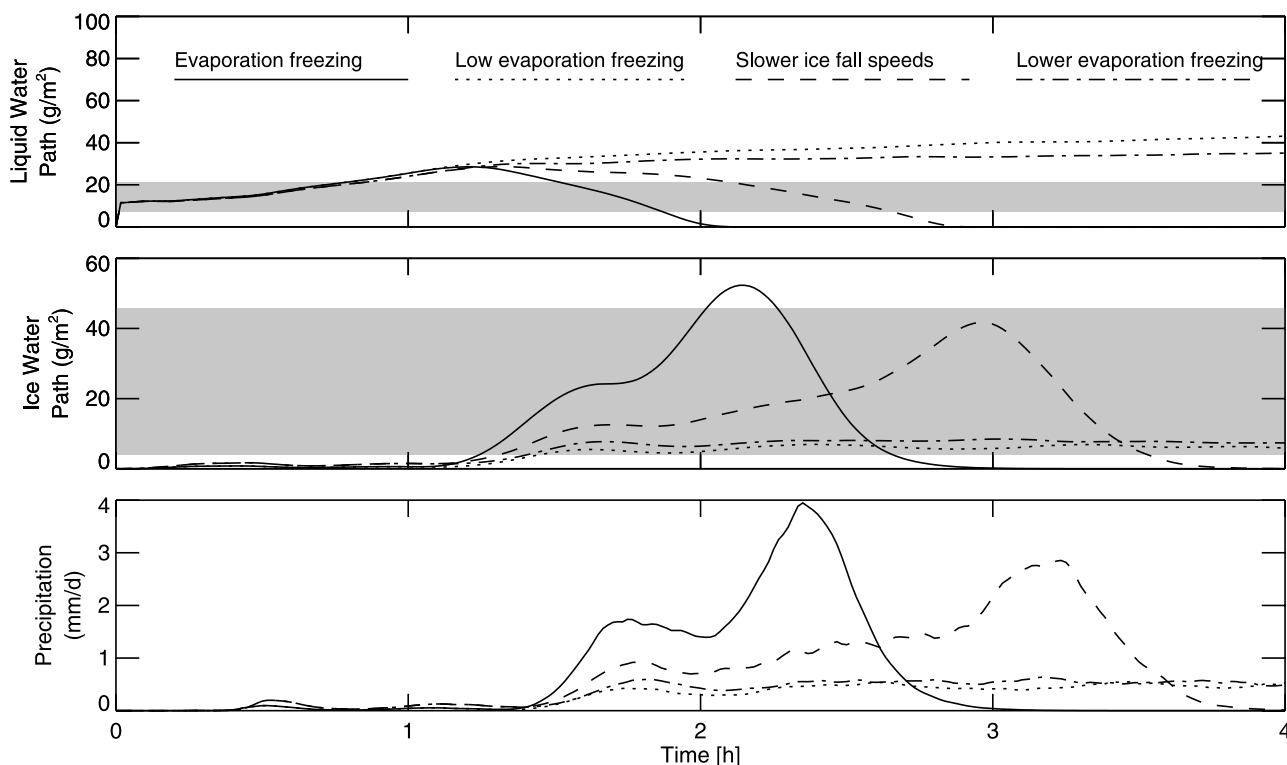


**Figure 14.** Time series of simulated domain-average liquid and ice water path and surface precipitation from simulations with evaporation freezing (solid line), reduced rate of evaporation freezing (dotted line), in addition to reduced ice fall speeds (dashed line), in addition to further reduced rate of evaporation freezing (dash-dotted line), compared with the range derived from in situ observations during BASE flight 18A and the case 18 statistics presented by *Pinto and Curry* [2001] (shaded). Further details provided in section 4.4.

ditions, measured ice nuclei are not capable of accounting for measured ice, and ice multiplication processes cannot account for the difference.

[56] 2. Lowering assumed ice fall speeds can increase predicted ice mass, but predicted number concentrations of ice larger than  $53 \mu\text{m}$  in maximum dimension remain two orders of magnitude lower than measured, whereas measurement errors are expected to remain below about a factor of five.

[57] 3. In order to sustain ice mass in the observed range via standard heterogeneous nucleation modes, simulations require either (1) free tropospheric ice nucleus concentrations several orders of magnitude greater than measured or (2) an ocean source maintaining at least about  $6 \text{ L}^{-1}$  in the surface layer. The high concentrations of ice nuclei required, either above or below cloud, are unlikely to have gone undetected by the CFDC unless the nuclei were larger than  $1.5 \mu\text{m}$  in diameter or active only in the contact mode.

[58] 4. Proposed evaporation nuclei or evaporation freezing mechanisms could sustain ice mass and number in the observed range under M-PACE conditions if they transform roughly one in  $10^4$ – $10^5$  drops into ice nuclei (evaporation nuclei) or directly into ice crystals (evaporation freezing). If evaporation nuclei were active at  $-4^\circ\text{C}$  in the deposition mode or their activity were destroyed by heating, they would not have been detected by the CFDC.

[59] 5. It is also possible to sustain ice mass and number near the observed range with low rates of drop freezing per

unit volume or per unit surface area. Freezing in this manner could be explained by cloud-phase chemistry that exposes or creates biogenic ice nuclei or surfactant films with ice nucleating properties. If ice were directly nucleated from the drop phase in this manner, there would be no evidence measurable in the aerosol phase by the CFDC.

[60] 6. Simulations that severely underpredict the number concentrations of ice larger than  $53 \mu\text{m}$  in maximum dimension also underpredict glaciation of cloud-base regions. In our simulations, cloud base regions are most efficiently glaciated by freezing processes concentrated at cloud base: a surface source of easily activated nuclei, evaporation nuclei or evaporation freezing.

[61] 7. In simulations with contrasting BASE meteorology, the evaporation nuclei mechanism demonstrates a remarkable ability to maintain stable and long-lived mixed-phase layers over a wider range of conditions than the evaporation freezing mechanism. Such behavior is consistent with observations, but has been a challenge for modeling studies.

## 5. Discussion

[62] To evaluate our findings in a broader context, we have identified five general hypotheses that should be considered. First among these is that major dynamical aspects of the observed cloud fields are insufficiently reproduced by our modeling approach, preventing accurate

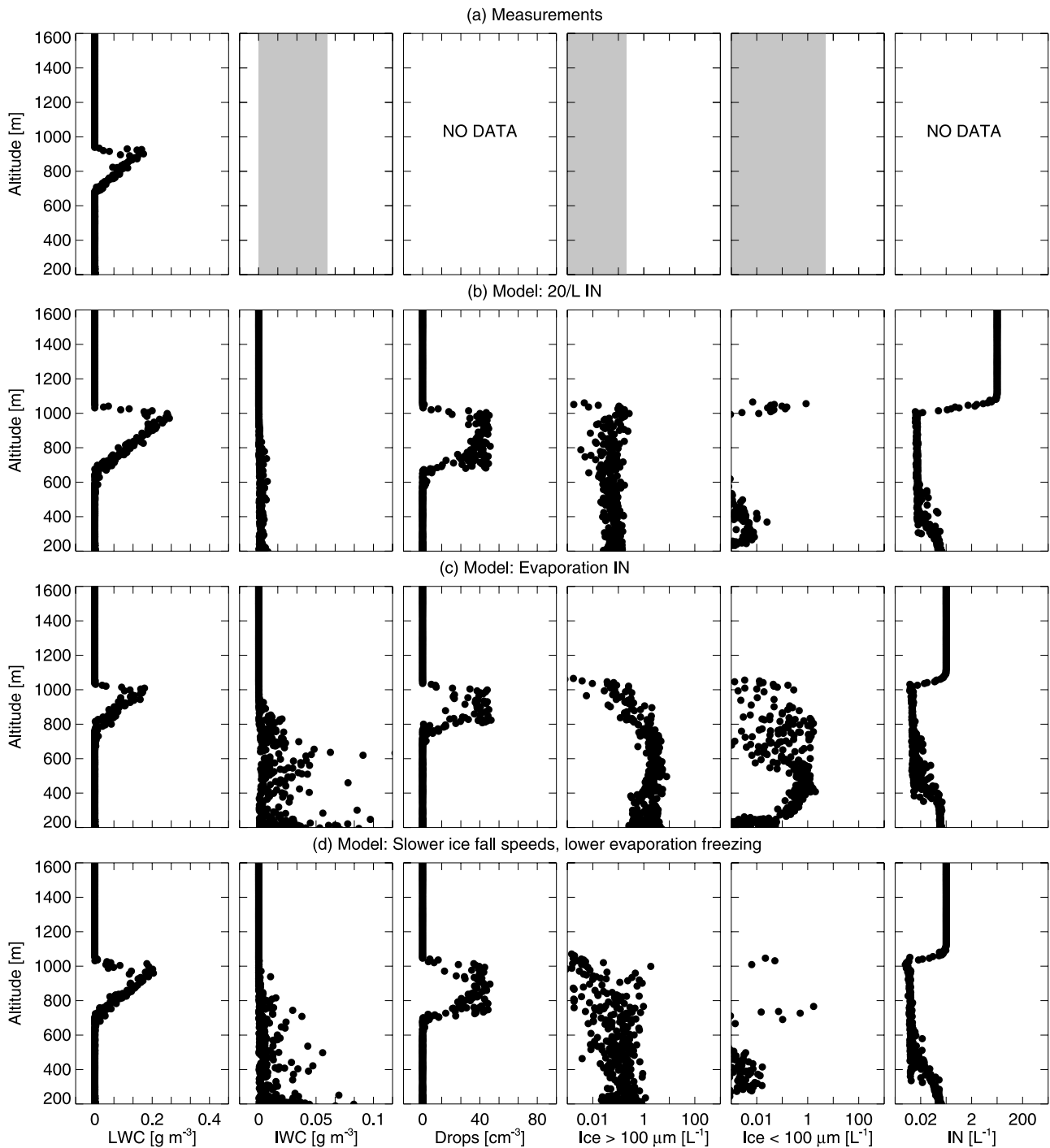


**Figure 15.** (a) BASE flight 18A measurements of liquid and ice water content, drop concentration, ice concentrations with maximum particle dimension larger and smaller than 100  $\mu\text{m}$  and unactivated ice nucleus (IN) concentration plotted as a function of altitude, compared with simulations with (b) 20/L ice nuclei aloft, (c) evaporation IN formation, and (d) slower ice fall speeds and a lower evaporation freezing rate. Measurements unavailable in archived data files are taken from previously published values [Pinto, 1998] (shaded). Model results are randomly sampled from the final field produced by each simulation (see Figures 13 and 14).

evaluation of microphysical processes. For instance, in a mesoscale modeling study of the same M-PACE time period that we consider here, Prenni *et al.* [2007] predict appreciable IWP only near the coast, which they attribute to enhanced entrainment of ice nuclei aloft associated with

coastal circulations. Since the Citation aircraft was unable to fly far from the coast for safety reasons (see Figure 1), we are unable to determine whether ice was primarily absent from clouds offshore, as Prenni *et al.* [2007] predict. However, Prenni *et al.* [2007] also predict maximum ice

number concentrations on the order of  $1 \text{ L}^{-1}$ , a factor of five higher than we are able to predict under any dynamical circumstances (with a background of  $0.2 \text{ L}^{-1}$  and no significant multiplication), leading us to believe that IWP would also be underpredicted near the coast in mesoscale simulations that used our baseline microphysical assumptions (as in the simulations we present here). Overall, we cannot fully evaluate this hypothesis with existing data and modeling tools; however, the close agreement between many of our simulation features and the full range of in situ observations leads us to believe that we likely represent observed cloud fields at least sufficiently to consider subsequent hypotheses.

[63] A second important hypothesis is that, although the cloud fields may be represented with sufficient accuracy by our modeling approach, ice breakup on aircraft instruments resulted in significant overcounting of ice with maximum dimension larger than  $53 \mu\text{m}$ . (Aside, we note that results are not sensitive to using a higher size threshold of  $100 \mu\text{m}$  to compare measurements and simulations.) If that were the case, our simulation with slower ice fall speeds (Figures 5, 6c, and 9c) might best represent actual field conditions, and the lack of full glaciation that we predict in lower cloud regions could be incorrect owing to other model inaccuracies, which are especially difficult to quantify for the drizzle process. However, the highest concentrations of ice larger than  $53 \mu\text{m}$  that we predict in that case remain about two orders of magnitude fewer than observed. While counting errors greater than a factor of four have not been found for particles that large [e.g., *Field et al.*, 2006; *McFarquhar et al.*, 2007], they have also not been well established for most aircraft instrument configurations.

[64] A third hypothesis, in the case that our cloud dynamics is adequate and the measurements used are free from major undiagnosed errors, is that the evaporation nucleation mechanism is operating under M-PACE conditions. We have considered this possibility on the basis of what remains the most detailed review to date regarding ice initiation in warm-base convective clouds [*Beard*, 1992]. A compelling feature of this mechanism is that long-lived mixed-phase cloud layers result when it is applied in a similar manner to simulations under M-PACE and BASE conditions, using the literature as guidance for the rate of freezing. One possible source of such nuclei could be the organic particles emitted from the ocean surface layer during bubble bursting, which can release colloidal solids from their polymer gel coatings upon acidification [*Leck and Bigg*, 2005]. Some combination of active collision-coalescence (combining more acidic and less acidic aerosol cores), cloud-phase oxidation of ambient gases, concentration of the dissolved acids during drop evaporation, and enhanced contact of exposed solids with the surfaces of evaporating drops [*Durant and Shaw*, 2005] could help explain the correlation of ice production with the number of large droplets. Biologically active ocean waters have been associated with enhanced ice nucleus concentrations in the Arctic and elsewhere [*Schnell and Vali*, 1976; *Bigg*, 1996; *Szyrmer and Zawadzki*, 1997], the additional presence of sulfate has been hypothesized to be an “integral part” of the ice nucleating particles in such regions [*Rosinski et al.*, 1987], and it has been conjectured that these findings might be related to the possible presence of evaporation nuclei

[*Rosinski et al.*, 1987; *Bigg*, 1996]. We defer here to the closing words of the *Beard* [1992] review: “. . . the nature of evaporation nuclei and the circumstance under which they form must be determined from well-designed observational, laboratory and theoretical studies.” Since that was written, we are aware of no published work devoted to studying possible ice nucleation on drop residuals, aside from theoretical calculations aiming to determine whether electrical effects on scavenging of such nuclei could be the cause for the widely observed association of ice enhancement with the concentration of drops larger than  $20 \mu\text{m}$  in diameter. Aside, we note that those theoretical results remain divided, with earlier results indicating that larger drops are more likely to electroscavenge evaporation nuclei [*Tinsley et al.*, 2000, 2001], but later results indicating that smaller drops will scavenge more efficiently [*Tripathi and Harrison*, 2002]; we have used the later results here simply because they are the most recent in the developing literature.

[65] A fourth hypothesis is that drops do freeze anomalously (nonhomogeneously) during the evaporation process. At least two possible reasons for such behavior have been suggested: (1) ice nucleation by long-chain organic compounds [e.g., *Bigg*, 1996; *Cantrell and Robinson*, 2006] that may be concentrated or uniquely oriented at drop surfaces during evaporation and may also have been accumulated by various possible means during the drop lifetime and (2) passage through a eutectic point of the hydrate of an abundant dissolved salt [e.g., *Korolev et al.*, 2003]. The latter possibility should probably be ruled out under M-PACE conditions since the eutectic points of sodium chloride and ammonium sulfate solutions occur at about  $-21$  and  $-18^\circ\text{C}$  respectively [*Rodebush*, 1918; *Kaufman*, 1960] (colder than in-cloud temperatures), but the ocean surface layer itself (via bubble-bursting emissions of aerosols) or cloud-processing of ambient gases could be sources of surface active organic species. Nonhomogeneous drop freezing has also been invoked to explain anomalous ice production observed in the evaporation zone of wave clouds in the  $-10$  to  $-35^\circ\text{C}$  temperature range [*Field et al.*, 2001; *Cotton and Field*, 2002; *Hegg and Noone*, 2005; *Baker and Lawson*, 2006], where it has been argued that evaporation nucleus formation is a less likely explanation [*Baker and Lawson*, 2006]. Whereas homogeneous ice nucleation rates rise extremely quickly with decreasing temperature, wave cloud observations can exhibit a much weaker dependence of peak apparent nucleation rate on decreasing temperature [*Field et al.*, 2001]. Laboratory measurements indicate that an idealized organic film can induce nucleation rates with remarkably weak temperature dependence, as well as the expected surface area dependence upon increasing drop size [*Zobrist et al.*, 2007]. Wave cloud measurements have also led to the suggestion that both aerosol properties and dynamical conditions (increasing downdraft strength) may influence apparent ice nucleation rates [*Hegg and Noone*, 2005].

[66] A fifth hypothesis is that we are missing unknown microphysical processes or misrepresenting known processes (such as fragmentation during ice-ice collisions or rime-splintering). These processes could include in-cloud chemistry that exposes or produces ice nuclei or surfactant films with ice nucleating properties [e.g., *Bigg*, 1996; *Leck and Bigg*, 2005; *Cantrell and Robinson*, 2006; *Zobrist et al.*,

2007, and references contained therein], and we find that low induced freezing rates per unit drop volume or per unit drop surface area could also sustain long-lived mixed-phase clouds consistent with many aspects of the M-PACE measurements. *Leck and Bigg* [2005] have also noted that condensation of oxidized sulfate gases directly upon aerosol surfaces can expose biogenic marine solids; if the resulting particles were easily activated ice nuclei and sufficient acidic gases were present to create them above cloud base, they could provide another in-cloud source of ice nuclei that would not build up to detectable concentrations in the aerosol phase. Briefly considering mixed-phase clouds in general, from the standpoint of widespread observations, it has been noted that there is a remarkably poor correlation between ice number concentration and temperature that remains unexplained [e.g., *Hobbs and Rangno*, 1985; *Fleishauer et al.*, 2002; *Korolev et al.*, 2003]; in contrast, over a wide range of stratus and cumulus cloud types with tops colder than about  $-6^{\circ}\text{C}$ , the strongest predictor for ice formation appears to be the presence of drops larger than about  $20\ \mu\text{m}$  in diameter, and the onset of ice enhancement also appears to be associated with entrainment of ambient air [*Mossop et al.*, 1972; *Hobbs and Rangno*, 1985]. While most clouds with significant vertical development are subject to much greater entrainment rates than the stratocumulus encountered during M-PACE, boundary layer cloud downdrafts do produce similar zones of rapid evaporation. The case we present here also exhibits high concentrations of large drops, whose role remains a mystery. Could they be a proxy for other factors, such as aerosol properties or an active collision-coalescence process? Ice-ice collisions and contact nucleation also remain poorly understood. Ice-liquid or ice-ice multiplication mechanisms may need to be faster than rime splintering in order to explain ice enhancement in cumuliform clouds [*Rangno and Hobbs*, 1991] and they probably cannot explain ice observations in wave clouds [*Cotton and Field*, 2002]. More recent observational surveys have suggested that the lack of correlation between ice particle number concentration and temperature points to the likelihood of a “universal mechanism” for which no explanation currently exists, although evaporation nuclei and evaporation freezing are candidates [*Korolev et al.*, 2003]. The M-PACE case demonstrates that a mechanism such as eutectic point freezing may not be universal enough to include the warmest temperatures, but cloud-phase chemistry could be an alternative.

[67] How best to evaluate these last three hypotheses? The fact that a wide range of possibilities can be found to explain the M-PACE observations relatively well, e.g., a surface source of ice nuclei not detectable by the CFDC, evaporation nuclei that are active at warm temperatures, evaporation freezing, or even low rates of freezing per unit drop volume or surface area, demonstrates that additional measurements are required to understand whether and how such mechanisms might work. Because it is increasingly evident that the composition of natural aerosols and cloud drops is often profoundly complex, one way to directly evaluate the third and fourth hypotheses would be to make measurements that operate upon real cloud drops, each of which has formed upon one such complex aerosol and has likely undergone at least some degree of subsequent transformation from processes such as scavenging of ambient

gases and other aerosol and cloud particles. Just as the CFDC probes the aerosol phase for ice nuclei, an instrument could be developed to measure freezing rates during the controlled evaporation of natural cloud drops under supercooled conditions. If supercooling is sufficient, some freezing would be expected from immersion and contact nuclei. Immersion nucleation rates should be consistent with interpretation of CFDC measurements. Contact nucleation rates, which are not currently measured during field programs despite their conjectured importance [e.g., *Morrison et al.*, 2005], should be enhanced during the evaporation process for some sizes of nuclei and drops [e.g., *Slinn and Hales*, 1971; *Pruppacher and Klett*, 1997]. If ambient aerosols are removed from the droplet stream during the measurement process, subsequent freezing would be an indication of evaporation nuclei, evaporation freezing or other processes. Cloud condensation nuclei and CFDC measurement techniques provide examples of instruments that are designed to emulate a mechanism of cloud particle formation for the purposes of counting. Cloud chambers are an alternative to new instrument development that may be less easily integrated into current aircraft studies, but they have been airborne with intriguing results [e.g., *Beard*, 1992]. Such process-oriented studies of natural cloud drops could serve to efficiently evaluate ice formation mechanisms that are not reliant on multiplication processes.

## Appendix A: Model Representation of Prognostic Ice Nuclei

[68] In each grid cell, ice nuclei are stored in an array of length  $K$  from most to least easily nucleated, such that total ice nuclei in each grid cell,  $N$ , are the sum

$$N = \sum_{i=1}^K N_i. \quad (\text{A1})$$

[69] In addition to advection, subsidence, and turbulent transport, each array element in each grid cell is then subject to possible sinks and sources

$$\frac{\partial N_i}{\partial t} = \underbrace{\left( -\frac{\partial N_{i,\text{cont}}}{\partial t} - \frac{\partial N_{i,\text{cond}}}{\partial t} - \frac{\partial N_{i,\text{dep}}}{\partial t} - \frac{\partial N_{i,\text{imm}}}{\partial t} \right)}_{\text{sinks}} + \underbrace{\left( \frac{\partial N_{i,\text{evap}}}{\partial t} + \frac{\partial N_{i,\text{surf}}}{\partial t} + \frac{\partial N_{i,\text{recyc}}}{\partial t} \right)}_{\text{sources}}, \quad (\text{A2})$$

where the terms are as follows.

[70] First, the rate of ice nucleus consumption in the contact mode in each array element is determined by the product of the number of ice nuclei available in that array element and a summation

$$\frac{\partial N_{i,\text{cont}}}{\partial t} = \left\{ \begin{array}{ll} N_i \cdot T < T_{\text{max,cont}} - (i-1)(T_{\text{max,cont}} - T_{\text{min,cont}})/K & \\ 0 & \text{otherwise} \end{array} \right\} \cdot \sum N_d C_{\text{scav}}. \quad (\text{A3})$$

where  $N_d$  is the number of drops of each size and  $C_{\text{scav}}$  is the rate at which drops of that size would scavenge nuclei (here assumed to be  $0.5 \mu\text{m}$  in diameter), which in turn depends upon the phoretic forces on nuclei near drops of each size in that grid cell. Using the formulations provided by Young [1974], for each drop size, we first calculate all phoretic coefficient elements except deviations of drop surface temperature and vapor pressure from the initial environmental profile at the start of each simulation; this is the part of the phoretic kernel that can be considered nearly constant at each elevation as a function of the sizes of the interacting particles. During the simulation, as vapor is condensing upon or evaporating from drops of various sizes in each grid cell, we then use the local deviation of temperature and vapor pressure over each drop size to calculate final ice nucleus scavenging rates, adding phoretic and Brownian components. In the contact mode, ice nuclei are arrayed from most easily nucleated ( $i = 1$ ) to least easily nucleated ( $i = K$ ) in terms of linear temperature change, where the values of limits  $T_{\text{max,cont}}$  and  $T_{\text{min,cont}}$  are listed in Table 1.

[71] Condensation nuclei are also arrayed from most to least easily nucleated in terms of linear temperature change, but vapor must also be supersaturated with respect to liquid water in order to generate a positive loss rate

$$\frac{\partial N_{i,\text{cond}}}{\partial t} = \begin{cases} N_i & S_w > 0, T < T_{\text{max,cond}} - (i-1)(T_{\text{max,cond}} - T_{\text{min,cond}})/K \\ 0 & \text{otherwise} \end{cases} / \Delta t. \quad (\text{A4})$$

where  $S_w$  is supersaturation with respect to water and  $\Delta t$  is the microphysical time step. For numerical efficiency, when condensation nuclei are available in a grid cell under such conditions, they are thus consumed instantly by creation of an ice crystal in the smallest ice size bin without passing through a short-lived early drop activation process.

[72] Activation of deposition nuclei requires water vapor supersaturation with respect to ice, and the nuclei are then arrayed in terms of ice supersaturation rather than temperature, which must simply exceed a minimum threshold (see Table 1) in order to generate a loss rate,

$$\frac{\partial N_{i,\text{dep}}}{\partial t} = \begin{cases} N_i & T < 0, S_i > 0.2((i-1)/K)^{1/4.39} \\ 0 & \text{otherwise} \end{cases} / \Delta t, \quad (\text{A5})$$

based on the simple relation shown by Pruppacher and Klett [1997, cf. Figure 9-20].

[73] Immersion nuclei are linearly arrayed with nucleation temperature, but their rate of activation loss depends upon the fraction of drops of each size that contain a nucleus,  $f_{\text{imm}}$ , such that

$$\frac{\partial N_{i,\text{imm}}}{\partial t} = \begin{cases} N_i & T < T_{\text{max,imm}} - (i-1)(T_{\text{max,imm}} - T_{\text{min,imm}})/K \\ 0 & \text{otherwise} \end{cases} \cdot \frac{\sum f_{\text{imm}} N_d}{\Delta t}. \quad (\text{A6})$$

[74] To calculate  $f_{\text{imm}}$  in each drop size bin, the total ‘‘aerosol cores’’ in each grid cell are first estimated as a weighted sum over the drops, where drops smaller than  $10 \mu\text{m}$  in radius are assumed to carry one aerosol core and the number of aerosol cores carried by larger drops is assumed to be the mean aerosol mass within drops of that size (a prognostic model variable) divided by the mean aerosol mass in a  $10 \mu\text{m}$  drop. Immersion nuclei are then assumed evenly distributed among the aerosol cores inside drops; larger drops are then more likely to freeze ( $f_{\text{imm}}$  is higher in those size bins), but the total number of nuclei consumed is limited to those available.

[75] Sources are generally not present aside from transport (as from subsidence aloft). However, simulations with evaporation nuclei include a source that is a small fraction  $f_{\text{evap}}$  of the rate of drops evaporating in that grid cell (see section 3.4),

$$\frac{\partial N_{i,\text{evap}}}{\partial t} = \begin{cases} f_{\text{evap}} \frac{\partial N_{d,\text{evap}}}{\partial t} & i = 1 \\ 0 & \text{otherwise,} \end{cases} \quad (\text{A7})$$

where all evaporation nuclei are assumed to populate the most easily nucleated class ( $i = 1$ ).

[76] A surface source of ice nuclei, when assumed to occur, is represented as

$$\frac{\partial N_{i,\text{surf}}}{\partial t} \text{ such that } \begin{cases} N_i = \text{constant} & i = 1, z < 100\text{m} \\ 0 & \text{otherwise,} \end{cases} \quad (\text{A8})$$

such that all source nuclei are assumed to be in the most easily activated class.

[77] Finally, sensitivity tests that describe recycling include a term for full ice nucleus recovery from the rate of evaporating ice crystals,

$$\frac{\partial N_{i,\text{recyc}}}{\partial t} = \begin{cases} \frac{\partial N_{i,\text{evap}}}{\partial t} & i = 1 \\ 0 & \text{otherwise,} \end{cases} \quad (\text{A9})$$

where the preactivated nuclei are again assumed to populate only the most easily activated array element.

[78] **Acknowledgments.** This research was supported by the DOE Office of Science, Office of Biological and Environmental Research, through Interagency Agreement DE-AI02-06ER64173 and contract DE-FG03-02ER63337. M-PACE data were obtained from the ARM Program archive, sponsored by the DOE Office of Science, Office of Biological and Environmental Research, Environmental Science Division. BASE data were obtained from the National Center for Atmospheric Research (NCAR) Research Aviation Facility (RAF) archive. NCEP data were obtained from the National Oceanic and Atmospheric Administration’s National Weather Service archive. We gratefully acknowledge additional financial support from the NASA Radiation Sciences Program and computational support provided by the NASA Advanced Supercomputing Division. We are grateful for contributions from three anonymous reviewers.

## References

- Ackerman, A. S., O. B. Toon, and P. V. Hobbs (1995), A model for particle microphysics, turbulent mixing, and radiative transfer in the stratocumulus-topped marine boundary layer and comparisons with measurements, *J. Atmos. Sci.*, *52*, 1204–1236.
- Ackerman, A. S., O. B. Toon, D. E. Stevens, A. J. Heymsfield, V. Ramanathan, and E. J. Welton (2000), Reduction of tropical cloudiness by soot, *Nature*, *288*, 1042–1047.
- Bacon, N. J., B. D. Swanson, M. B. Baker, and E. J. Davis (1998), Breakup of levitated frost particles, *J. Geophys. Res.*, *103*, 13,763–13,775.
- Baker, B. A., and R. P. Lawson (2006), In situ observations of the microphysical properties of wave, cirrus, and anvil clouds. Part I: Wave clouds, *J. Atmos. Sci.*, *63*, 3160–3185.
- Barth, M. C., et al. (2007), Cloud-scale model intercomparison of chemical constituent transport in deep convection, *Atmos. Chem. Phys.*, *7*, 4709–4731.
- Beard, K. V. (1992), Ice initiation in warm-base convective clouds: An assessment of microphysical mechanisms, *Atmos. Res.*, *28*, 125–152.
- Beard, K. V., and H. T. Ochs (1984), Collection and coalescence efficiencies for accretion, *J. Geophys. Res.*, *89*, 7165–7169.
- Beard, K. V., H. T. Ochs, and C. H. Twohy (2004), Aircraft measurements of high average charges on cloud drops in layer clouds, *Geophys. Res. Lett.*, *31*, L14111, doi:10.1029/2004GL020465.
- Beheng, K. D. (1987), Microphysical properties of glaciating cumulus clouds: Comparison of measurements with a numerical simulation, *Q. J. R. Meteorol. Soc.*, *113*, 1377–1382.
- Bigg, E. K. (1996), Ice forming nuclei in the high Arctic, *Tellus, Ser. B*, *48*, 223–233.
- Bigg, E. K., and C. Leck (2001), Cloud active particles over the central Arctic Ocean, *J. Geophys. Res.*, *106*, 32,155–32,166.
- Brownscombe, J. L., and N. S. C. Thorndike (1968), Freezing and shattering of water droplets in free fall, *Nature*, *220*, 687–689.
- Brutsaert, W. (1975), On a derivable formula for longwave radiation from clear skies, *Water Resour. Res.*, *11*, 742–744.
- Cantrell, W., and A. Heymsfield (2005), Production of ice in tropospheric clouds: A review, *Bull. Am. Meteorol. Soc.*, *86*, 795–807.
- Cantrell, W., and C. Robinson (2006), Heterogeneous freezing of ammonium sulfate and sodium chloride solutions by long chain alcohols, *Geophys. Res. Lett.*, *33*, L07802, doi:10.1029/2005GL024945.
- Cober, S. G., G. A. Isaac, A. V. Korolev, and J. W. Strapp (2001), Assessing cloud-phase conditions, *J. Appl. Meteorol.*, *40*, 1967–1983.
- Connolly, P. J., M. J. Flynn, Z. Ulanowski, T. W. Choullarton, M. W. Gallagher, and K. N. Bower (2007), Calibration of the cloud particle imager probes using calibration beads and ice crystal analogues: The depth of field, *J. Atmos. Oceanic Technol.*, in press.
- Cotton, R. J., and P. R. Field (2002), Ice nucleation characteristics of an isolated wave cloud, *Q. J. R. Meteorol. Soc.*, *128*, 2417–2437.
- Curry, J. A. (2001), Introduction to special section: FIRE Arctic Clouds Experiment, *J. Geophys. Res.*, *106*, 14,985–14,987.
- Curry, J. A., W. B. Rossow, D. Randall, and J. L. Schramm (1996), Overview of Arctic cloud and radiation characteristics, *J. Clim.*, *9*, 1731–1764.
- Curry, J. A., J. O. Pinto, T. Benner, and M. Tschudi (1997), Evolution of the cloudy boundary layer during the autumnal freezing of the Beaufort Sea, *J. Geophys. Res.*, *102*, 13,851–13,860.
- Curry, J. A., et al. (2000), FIRE Arctic Clouds Experiment, *Bull. Am. Meteorol. Soc.*, *81*, 5–29.
- DeMott, P. J., D. J. Cziczo, A. J. Prenni, D. M. Murphy, S. M. Kreidenweis, D. S. Thomson, R. Borsys, and D. C. Rogers (2003a), Measurements of the concentration and composition of nuclei for cirrus formation, *Proc. Natl. Acad. Sci. U. S. A.*, *100*, 14,655–14,660, doi:10.1073/pnas.2532677100.
- DeMott, P. J., K. Sassen, M. R. Poellot, D. Baumgardner, D. C. Rogers, S. D. Brooks, A. J. Prenni, and S. M. Kreidenweis (2003b), African dust aerosols as atmospheric ice nuclei, *Geophys. Res. Lett.*, *30*(14), 1732, doi:10.1029/2003GL017410.
- Durant, A. J., and R. A. Shaw (2005), Evaporation freezing by contact nucleation inside-out, *Geophys. Res. Lett.*, *32*, L20814, doi:10.1029/2005GL024175.
- Field, P. R., et al. (2001), Ice nucleation in orographic wave clouds: Measurements made during INTACC, *Q. J. R. Meteorol. Soc.*, *127*, 1493–1512.
- Field, P. R., R. Wood, P. R. A. Brown, P. H. Kaye, E. Hirst, R. Greenaway, and J. A. Smith (2003), Ice particle interarrival times measured with a fast FSSP, *J. Atmos. Oceanic Technol.*, *20*, 249–261.
- Field, P. R., A. J. Heymsfield, and A. Bansemer (2006), Shattering and particle interarrival times measured by optical array probes in ice clouds, *J. Atmos. Oceanic Technol.*, *23*, 1357–1371.
- Fleishauer, R. P., V. E. Larson, and T. H. Vonder Haar (2002), Observed microphysical structure of midlevel, mixed-phase clouds, *J. Atmos. Sci.*, *59*, 1779–1804.
- Fountain, A. G., and T. Ohtake (1985), Concentrations and source areas of ice nuclei in the Alaskan atmosphere, *J. Clim. Appl. Meteorol.*, *24*, 377–382.
- Fridlind, A. M., M. Z. Jacobson, V.-M. Kerminen, R. E. Hillamo, V. Ricard, and J.-L. Jaffrezo (2000), Analysis of gas-aerosol partitioning in the Arctic: Comparison of size-resolved equilibrium model results with field data, *J. Geophys. Res.*, *105*, 19,891–19,904.
- Gayet, J.-F., G. Febvre, and H. Larsen (1996), The reliability of the PMS FSSP in the presence of small ice crystals, *J. Atmos. Oceanic Technol.*, *13*, 1300–1310.
- Hall, W. D. (1980), A detailed microphysical model within a two-dimensional model framework: Model description and preliminary results, *J. Atmos. Sci.*, *37*, 2486–2507.
- Hallett, J., and S. C. Mossop (1974), Production of secondary ice particles during the riming process, *Nature*, *249*, 26–28.
- Harrington, J. Y., and P. Q. Olsson (2001), On the potential influence of ice nuclei on surface-forced marine stratocumulus cloud dynamics, *J. Geophys. Res.*, *106*, 27,473–27,484.
- Harrington, J. Y., T. Reisin, W. R. Cotton, and S. M. Kreidenweis (1999), Cloud resolving simulations of Arctic stratus, part II: Transition-season clouds, *Atmos. Res.*, *51*, 45–75.
- Harrison, R. G., and K. S. Carslaw (2003), Ion-aerosol-cloud processes in the lower atmosphere, *Rev. Geophys.*, *41*(3), 1012, doi:10.1029/2002RG000114.
- Hegg, D. A., and K. J. Noone (2005), Phenomenology of ice formation in INTACC and SUCCESS, *Atmos. Res.*, *78*, 33–45.
- Heymsfield, A. J., and M. Kajikawa (1987), An improved approach to calculating terminal velocities of plate-like crystals and graupel, *J. Atmos. Sci.*, *44*, 1088–1099.
- Heymsfield, A. J., and S. C. Mossop (1984), Temperature dependence of secondary ice crystal production during soft hail growth by riming, *Q. J. R. Meteorol. Soc.*, *110*, 765–770.
- Hobbs, P. V. (1969), Ice multiplication in clouds, *J. Atmos. Sci.*, *26*, 315–318.
- Hobbs, P. V., and A. J. Alkezweeny (1968), The fragmentation of freezing water droplets in free fall, *J. Atmos. Sci.*, *25*, 881–888.
- Hobbs, P. V., and A. L. Rangno (1985), Ice particle concentrations in clouds, *J. Atmos. Sci.*, *42*, 2523–2549.
- Hobbs, P. V., and A. L. Rangno (1998), Microstructures of low and middle-level clouds over the Beaufort Sea, *Q. J. R. Meteorol. Soc.*, *124*, 2035–2071.
- Jacobson, M. Z., R. P. Turco, E. J. Jensen, and O. B. Toon (1994), Modeling coagulation among particles of different composition and size, *Atmos. Environ., Part A*, *28*, 1327–1338.
- Jensen, E. J., et al. (1998), Ice nucleation processes in upper tropospheric wave-clouds observed during SUCCESS, *Geophys. Res. Lett.*, *25*, 1363–1366.
- Jiang, H., W. R. Cotton, J. O. Pinto, J. A. Curry, and M. J. Weissbluth (2000), Cloud resolving simulations of mixed-phase Arctic stratus observed during BASE: Sensitivity to concentration of ice crystals and large-scale heat and moisture advection, *J. Atmos. Sci.*, *57*, 2105–2117.
- Kärcher, B., and T. Koop (2005), The role of organic aerosols in homogeneous ice formation, *Atmos. Chem. Phys.*, *5*, 703–714.
- Kaufman, D. W. (1960), Low temperature properties and uses of salt and brine, in *Sodium Chloride: The Production and Properties of Salt and Brine*, *Am. Chem. Soc. Monogr. Ser.*, vol. 145, edited by D. W. Kaufman, chap. 23, pp. 547–568, Reinhold, New York.
- Kirkpatrick, M. P., A. S. Ackerman, D. E. Stevens, and N. N. Mansour (2006), On the application of the dynamic Smagorinsky model to large-eddy simulations of the cloud-topped atmospheric boundary layer, *J. Atmos. Sci.*, *63*, 526–546.
- Knopf, D. A., and T. Koop (2006), Heterogeneous nucleation of ice on surrogates of mineral dust, *J. Geophys. Res.*, *111*, D12201, doi:10.1029/2005JD006894.
- Koop, T., B. Luo, A. Tsias, and T. Peter (2000), Water activity as the determinant for homogeneous ice nucleation in aqueous solutions, *Nature*, *406*, 611–614.
- Korolev, A. V., and G. A. Isaac (1999), Ice particle habits in Arctic clouds, *Geophys. Res. Lett.*, *26*, 1299–1302.
- Korolev, A. V., G. A. Isaac, S. G. Cober, J. W. Strapp, and J. Hallett (2003), Microphysical characterization of mixed-phase clouds, *Q. J. R. Meteorol. Soc.*, *129*, 39–65.
- Leck, C., and E. K. Bigg (2005), Source and evolution of the marine aerosol—A new perspective, *Geophys. Res. Lett.*, *32*, L19803, doi:10.1029/2005GL023651.
- Mason, B. J., and J. Maybank (1958), Ice-nucleating properties of some natural mineral dusts, *Q. J. R. Meteorol. Soc.*, *84*, 235–241.
- McFarquhar, G. M., and S. G. Cober (2004), Single-scattering properties of mixed-phase Arctic clouds at solar wavelengths: Impacts on radiative transfer, *J. Clim.*, *17*, 3799–3813.
- McFarquhar, G. M., G. Zhang, M. Poellot, G. Kok, R. McCoy, T. Tooman, A. Fridlind, and A. J. Heymsfield (2007), Ice properties of single-layer

- stratocumulus during the Mixed-Phase Arctic Cloud Experiment: 1. Observations, *J. Geophys. Res.*, doi:10.1029/2007JD008633, in press.
- Morrison, H., M. D. Shupe, J. O. Pinto, and J. A. Curry (2005), Possible roles of ice nucleation mode and ice nuclei depletion in the extended lifetime of Arctic mixed-phase clouds, *Geophys. Res. Lett.*, *32*, L18801, doi:10.1029/2005GL023614.
- Mossop, S. C. (1970), Concentrations of ice crystals in clouds, *Bull. Am. Meteorol. Soc.*, *51*, 474–479.
- Mossop, S. C. (1985), The origin and concentration of ice crystals in clouds, *Bull. Am. Meteorol. Soc.*, *66*, 264–273.
- Mossop, S. C., and J. Hallett (1974), Ice crystal concentration in cumulus clouds: Influence of the drop spectrum, *Science*, *186*, 632–634.
- Mossop, S. C., R. E. Ruskin, and K. J. Heffernan (1968), Glaciation of a cumulus at approximately  $-4^{\circ}\text{C}$ , *J. Atmos. Sci.*, *25*, 889–899.
- Mossop, S. C., R. E. Cottis, and B. M. Bartlett (1972), Ice crystal concentrations in cumulus and stratocumulus clouds, *Q. J. R. Meteorol. Soc.*, *98*, 105–123.
- Olsson, P. Q., and J. Y. Harrington (2000), Dynamics and energetics of the cloudy boundary layer in simulations of off-ice flow in the marginal ice zone, *J. Geophys. Res.*, *105*, 11,889–11,899.
- Oraltay, R. G., and J. Hallett (1989), Evaporation and melting of ice crystals: A laboratory study, *Atmos. Res.*, *24*, 169–189.
- Oraltay, R. G., and J. Hallett (2005), The melting layer: A laboratory investigation of ice particle melt and evaporation near  $0^{\circ}\text{C}$ , *J. Appl. Meteorol.*, *44*, 206–220.
- Ovtchinnikov, M., Y. L. Kogan, and A. M. Blyth (2000), An investigation of ice production mechanisms in small cumuliiform clouds using a 3D model with explicit microphysics. Part II: Case study of New Mexico cumulus clouds, *J. Atmos. Sci.*, *57*, 3004–3020.
- Pinto, J. O. (1998), Autumnal mixed-phase cloudy boundary layers in the Arctic, *J. Atmos. Sci.*, *55*, 2016–2038.
- Pinto, J. O., and J. A. Curry (2001), Cloud-aerosol interactions during autumn over Beaufort Sea, *J. Geophys. Res.*, *106*, 15,077–15,097.
- Prenni, A. J., J. Y. Harrington, M. Tjernström, P. J. DeMott, A. Avramov, C. N. Long, S. M. Kreidenweis, P. Q. Olsson, and J. Verlinde (2007), Can ice-nucleating aerosols affect Arctic seasonal climate?, *Bull. Am. Meteorol. Soc.*, *88*, 541–550, doi:10.1175/BAMS-88-4-541.
- Pruppacher, H. R., and J. D. Klett (1997), *Microphysics of Clouds and Precipitation*, 2nd ed., 954 pp., Springer, New York.
- Randall, D., et al. (1998), Status of and outlook for large-scale modeling of atmosphere-ice-ocean interactions in the Arctic, *Bull. Am. Meteorol. Soc.*, *79*, 197–219.
- Rangno, A. L., and P. V. Hobbs (1991), Ice particle concentration and precipitation development in small polar maritime cumuliiform clouds, *Q. J. R. Meteorol. Soc.*, *117*, 207–241.
- Rangno, A. L., and P. V. Hobbs (2001), Ice particles in stratiform clouds in the Arctic and possible mechanisms for the production of high ice concentrations, *J. Geophys. Res.*, *106*, 15,065–15,075.
- Roberts, P., and J. Hallett (1967), A laboratory study of the ice nucleating properties of some mineral particulates, *Q. J. R. Meteorol. Soc.*, *94*, 25–34.
- Rodebush, W. H. (1918), The freezing points of concentrated solutions and the free energy of solution of salts, *J. Am. Chem. Soc.*, *40*, 1204–1213.
- Rogers, D. C., P. J. DeMott, and S. M. Kreidenweis (2001a), Airborne measurements of tropospheric ice-nucleating aerosol particles in the Arctic spring, *J. Geophys. Res.*, *106*, 15,053–15,063.
- Rogers, D. C., P. J. DeMott, S. M. Kreidenweis, and Y. Chen (2001b), A continuous-flow diffusion chamber for airborne measurements of ice nuclei, *J. Atmos. Oceanic Technol.*, *18*, 725–741.
- Rosinski, J., and G. Morgan (1991), Cloud condensation nuclei as a source of ice-forming nuclei in clouds, *J. Aerosol Sci.*, *22*, 123–133.
- Rosinski, J., P. L. Haagenson, C. T. Nagamoto, and F. Parungo (1987), Nature of ice-forming nuclei in marine air masses, *J. Aerosol Sci.*, *18*, 291–309.
- Schnell, R. C., and G. Vali (1976), Biogenic ice nuclei: Part I. Terrestrial and marine sources, *J. Atmos. Sci.*, *33*, 1554–1564.
- Shupe, M. D., S. Y. Matrosov, and T. Uttal (2006), Arctic mixed-phase cloud properties derived from surface-based sensors at SHEBA, *J. Atmos. Sci.*, *63*, 697–711.
- Slinn, W. G. N., and J. M. Hales (1971), A reevaluation of the role of thermophoresis as a mechanism of in- and below-cloud scavenging, *J. Atmos. Sci.*, *28*, 1465–1471.
- Stammes, K., R. G. Ellingson, J. A. Curry, J. E. Walsh, and B. D. Zak (1999), Review of science issues, deployment strategy, and status for the ARM North Slope of Alaska–Adjacent Arctic Ocean climate research site, *J. Clim.*, *12*, 46–63.
- Stevens, B., et al. (2001), Simulations of trade wind cumuli under a strong inversion, *J. Atmos. Sci.*, *58*, 1870–1891.
- Stevens, B., et al. (2005), Evaluation of large-eddy simulations via observations of nocturnal marine stratocumulus, *Mon. Weather Rev.*, *133*, 1443–1462, doi:10.1175/MWR2930.1.
- Stevens, D. E., and C. S. Bretherton (1996), A forward-in-time advection scheme and adaptive multilevel flow solver for nearly incompressible atmospheric flow, *J. Comput. Phys.*, *129*, 284–295.
- Stevens, D. E., A. S. Ackerman, and C. S. Bretherton (2002), Effects of domain size and numerical resolution on the simulation of shallow cumulus convection, *J. Atmos. Sci.*, *59*, 3285–3301.
- Strapp, J., F. Albers, A. Reuter, A. Korolev, U. Maixner, E. Rashke, and Z. Vukovic (2001), Laboratory measurements of the response of a PMS OAP-2DC, *J. Atmos. Oceanic Technol.*, *18*(7), 1150–1170.
- Szyrmer, W., and I. Zawadzki (1997), Biogenic and anthropogenic sources of ice-forming nuclei: A review, *Bull. Am. Meteorol. Soc.*, *78*, 209–228.
- Takahashi, T., Y. Nagao, and Y. Kushiya (1995), Possible high ice particle production during graupel-graupel collisions, *J. Atmos. Sci.*, *52*, 4523–4527.
- Tinsley, B. A., R. P. Rohrbaugh, M. Hei, and K. V. Beard (2000), Effects of image charges on the scavenging of aerosol particles by cloud droplets and on droplet charging and possible ice nucleation processes, *J. Atmos. Sci.*, *57*, 2118–2134.
- Tinsley, B. A., R. P. Rohrbaugh, and M. Hei (2001), Electroscavenging in clouds with broad droplet size distributions and weak electrification, *Atmos. Res.*, *59–60*, 115–135.
- Toon, O. B., C. P. McKay, T. P. Ackerman, and K. Santhaman (1989), Rapid calculation of radiative heating and photodissociation rates in inhomogeneous multiple scattering atmospheres, *J. Geophys. Res.*, *94*, 16,287–16,301.
- Tripathi, S. N., and R. G. Harrison (2002), Enhancement of contact nucleation by scavenging of charged aerosol particles, *Atmos. Res.*, *62*, 57–70.
- Vardiman, L. (1978), The generation of secondary ice particles in clouds by crystal-crystal collisions, *J. Atmos. Sci.*, *35*, 2168–2180.
- Verlinde, J., et al. (2007), The Mixed-Phase Arctic Cloud Experiment (M-PACE), *Bull. Am. Meteorol. Soc.*, *88*, 205–221, doi:10.1175/BAMS-88-2-205.
- Xie, S., S. A. Klein, J. J. Yio, A. C. M. Beljaars, C. N. Long, and M. Zhang (2006), An assessment of ECMWF analyses and model forecasts over the North Slope of Alaska using observations from the ARM Mixed-Phase Arctic Cloud Experiment, *J. Geophys. Res.*, *111*, D05107, doi:10.1029/2005JD006509.
- Young, K. C. (1974), The role of contact nucleation in ice phase initiation in clouds, *J. Atmos. Sci.*, *31*, 768–776.
- Zhou, J., E. Swietlicki, O. H. Berg, P. P. Aalto, K. Hameri, E. D. Nilsson, and C. Leck (2001), Hygroscopic properties of aerosol particles over the central Arctic Ocean during summer, *J. Geophys. Res.*, *106*, 32,111–32,124.
- Zobrist, B., T. Koop, B. P. Luo, C. Marcolli, and T. Peter (2007), Heterogeneous ice nucleation rate coefficient of water droplets coated by a nonadecanol monolayer, *J. Phys. Chem.*, *111*, 2149–2155.

A. S. Ackerman and A. M. Fridlind, NASA Goddard Institute for Space Studies, 2880 Broadway, New York, NY 10025, USA. (ann.fridlind@nasa.gov)

P. J. DeMott and A. J. Prenni, Department of Atmospheric Science, Colorado State University, Fort Collins, CO 80523, USA.

A. J. Heymsfield, National Center for Atmospheric Research, Boulder, CO 80307, USA.

G. McFarquhar and G. Zhang, Department of Atmospheric Sciences, University of Illinois, 105 S. Gregory Street, Urbana, IL 61801, USA.

M. R. Poellot, Department of Atmospheric Sciences, University of North Dakota, Grand Forks, ND 58202, USA.